Molecular Neurobiology (2022) 59:4159–4178
https://doi.org/10.1007/s12035-022-02838-y

Treatment with IFB-088 Improves Neuropathy in CMT1A and CMT1B Mice

Yunhong Bai[1] · Caroline Treins[2] · Vera G. Volpi[3] · Cristina Scapin[3] · Cinzia Ferri[3] · Rosa Mastrangelo[3] · Thierry Touvier[3] · Francesca Florio[3] · Francesca Bianchi[4] · Ubaldo Del Carro[4] · Frank F. Baas[5] · David Wang[1] · Pierre Miniou[2] · Philippe Guedat[2] · Michael E. Shy[1] · Maurizio D'Antonio[3]

Received: 23 December 2021 / Accepted: 9 April 2022 / Published online: 30 April 2022

Abstract

Charcot-Marie-Tooth disease type 1A (CMT1A), caused by duplication of the peripheral myelin protein 22 (*PMP22*) gene, and CMT1B, caused by mutations in myelin protein zero (*MPZ*) gene, are the two most common forms of demyelinating CMT (CMT1), and no treatments are available for either. Prior studies of the *Mpz*Ser63del mouse model of CMT1B have demonstrated that protein misfolding, endoplasmic reticulum (ER) retention and activation of the unfolded protein response (UPR) contributed to the neuropathy. Heterozygous patients with an arginine to cysteine mutation in MPZ (*MPZ*R98C) develop a severe infantile form of CMT1B which is modelled by *Mpz*R98C/+mice that also show ER stress and an activated UPR. C3-PMP22 mice are considered to effectively model CMT1A. Altered proteostasis, ER stress and activation of the UPR have been demonstrated in mice carrying *Pmp22* mutations. To determine whether enabling the ER stress/UPR and readjusting protein homeostasis would effectively treat these models of CMT1B and CMT1A, we administered Sephin1/IFB-088/icerguestat, a UPR modulator which showed efficacy in the *Mpz*S63del model of CMT1B, to heterozygous *Mpz*R98C and C3-PMP22 mice. Mice were analysed by behavioural, neurophysiological, morphological and biochemical measures. Both *Mpz*R98C/+and C3-PMP22 mice improved in motor function and neurophysiology. Myelination, as demonstrated by *g*-ratios and myelin thickness, improved in CMT1B and CMT1A mice and markers of UPR activation returned towards wild-type values. Taken together, our results demonstrate the capability of IFB-088 to treat a second mouse model of CMT1B and a mouse model of CMT1A, the most common form of CMT. Given the recent benefits of IFB-088 treatment in amyotrophic lateral sclerosis and multiple sclerosis animal models, these data demonstrate its potential in managing UPR and ER stress for multiple mutations in CMT1 as well as in other neurodegenerative diseases.

Keywords Charcot-Marie-Tooth · Neuropathy · Proteostasis · UPR · IFB-088/Sephin1/icerguestat

Abbreviations

AD	Autosomal dominant
AR	Autosomal recessive
ASO	Anti-sense oligonucleotides
ATF4	Activating transcription factor 4
BiP	Immunoglobulin heavy chain-binding protein
CHOP	C/EBP homologous protein
CMT	Charcot-Marie-Tooth
CMAP	Compound muscle action potential
DRG	Dorsal root ganglia
eIF2α	Alpha subunit of the eukaryotic translation initiation factor 2
ER	Endoplasmic reticulum
ERAD	ER-associated degradation
ERQC	Endoplasmic reticulum protein quality control

Michael E. Shy and Maurizio D'Antonio contributed equally to this work.

✉ Maurizio D'Antonio
dantonio.maurizio@hsr.it

[1] Department of Neurology, Carver College of Medicine, University of Iowa, Iowa City, IA 52242, USA

[2] InFlectis BioScience, 44300 Nantes, France

[3] Division of Genetics and Cell Biology, San Raffaele Scientific Institute DIBIT, 20132 Milan, Italy

[4] Division of Neuroscience, San Raffaele Scientific Institute DIBIT, 20132 Milan, Italy

[5] Department of Clinical Genetics, Leiden University Medical Center, Leiden, The Netherlands

Grp94	Glucose regulated protein 94
IRE1	Inositol-requiring enzyme 1
MBP	Myelin-binding protein
MPZ	Myelin protein zero
MNCV	Motor nerve conduction velocity
NCV	Nerve conduction velocity
NF	Neurofilament
PERK	Protein-kinase RNA-like endoplasmic reticulum kinase
PMP22	Peripheral myelin protein 22
PND	Post-natal day
PPP1R15A	Protein phosphatase 1 regulatory subunit 15A
PQC	Protein quality control
SNAP	Sensory nerve action potential
SNCV	Sensory nerve conduction velocity
UPR	Unfolded protein response
Tr^J	Trembler J
TEM	Transmission electron microscopy
WB	Western blot
WT	Wild type
XBP1	X-box-binding protein-1

Introduction

Charcot-Marie-Tooth (CMT) disease refers to heritable peripheral neuropathies, which are the most common genetic neuromuscular diseases, affecting 1:2500 individuals [1]. Autosomal dominant (AD) inheritance is the most common, followed by X-linked and autosomal recessive (AR) forms. Most forms of CMT are demyelinating while approximately one-third appear to be primary axonal disorders [2, 3]. CMT1A is the most common form, affecting approximately half of all patients with CMT [2], and is caused by a 1.4-Mb duplication within chromosome 17p11.2, in the region containing the peripheral myelin protein 22 (*PMP22*) gene [4, 5]. CMT1B (caused by mutations in the myelin protein zero (*MPZ*) gene, encoding for P0 protein) [6] is the second most frequent AD demyelinating form, encompassing around 5% of CMT cases [2]. At present, there are no effective treatments to slow progression or improve neuropathy in patients with CMT1A or CMT1B.

Experiments in cultured Schwann cells indicated that 80% of newly synthesized PMP22 is rapidly degraded by the proteasome under normal conditions, with only 20% reaching the cell surface or myelin sheath [7]. Whether this ratio is altered when PMP22 is over-expressed in CMT1A is unknown. Ordinarily, the maintenance of correct protein homeostasis is tightly controlled by protein quality control mechanisms [8]. The elevated protein expression associated with *PMP22* trisomy, in conjunction with the instability of the PMP22 protein, may impose a heavy burden on the endoplasmic reticulum (ER) protein quality control (ERQC) mechanisms [9–12]. When these control mechanisms fail, stress responses are activated leading to protein-kinase RNA–like endoplasmic reticulum kinase (PERK) (one of the unfolded protein response (UPR) sensors)–mediated phosphorylation of the alpha subunit of the eukaryotic translation initiation factor 2 (eIF2α) [13]. This phosphorylation causes an attenuation of global protein synthesis which reduces protein overload in the ER while allowing the translation of selected genes supporting stress recovery [14]. The extent to which these responses are activated in CMT1A is unclear, though there have been studies suggesting UPR activation in a CMT1A mouse model carrying seven copies of the human *PMP22* gene, the C22 mouse, which shows a severe dysmyelinating neuropathy [15], and in Trembler J (Tr^J) mice [16], which are caused by a missense mutation in *Pmp22* [17].

Over 200 different mutations in *MPZ* cause neuropathy (http://hihg.med.miami.edu/code/http/cmt/public_html/index.html#/), and the disease mechanisms are largely unknown. One group of mutations presents clinically in infancy or early childhood, with very slow nerve conduction velocities (NCV), and dysmyelination morphologically. Another group of *MPZ* mutations does not present clinically until adulthood, with near normal NCV, and axonal damage but minimal demyelination morphologically (sometimes called CMT2I or CMT2J) [18]. Several *MPZ* mutations in these groups have been shown in vitro to cause the accumulation of the mutant protein within the ER, where it triggered ER stress and activated the UPR. These included *Mpz* S51ΔW57 [19], 506delT and 550del3insG [20, 21]. Moreover, two mouse models of CMT1B, the *Mpz*Ser63del and *Mpz*R98C mice [22, 23], demonstrated ER retention of the mutant protein and a canonical UPR. The compound IFB-088 (icerguastat, also known as sephin1) was developed to prolong protein translation attenuation in response to stress by inhibiting eIF2α dephosphorylation to allow cells to restore cellular homeostasis [24]. Oral treatment with IFB-088 largely prevented the molecular, motor and morphological abnormalities of the neuropathy of *Mpz*Ser63del mice [24]. Whether treatment with IFB-088 is effective for only the Ser63del *MPZ* mutation is not known. This is an important question perhaps since as many as 40% of *MPZ* mutations have been recently shown to activate components of the UPR [20]. Accordingly, we elected to treat *Mpz*R98C/+ mice with IFB-088. We also hypothesized that IFB-088 may have effects on CMT1A, because of the highly metastable nature of PMP22 and because of UPR activity in C22 and Tr^J mice [15, 17]. We therefore chose to use IFB-088 to treat the C3-PMP22 mouse model of CMT1A. C3-PMP22 mice, which carry 3–4 copies of the human *PMP22* gene, develop a slowly progressive dysmyelinating peripheral neuropathy that is thought to be an appropriate model of CMT1A [25, 26]. Both CMT1B and CMT1A models were treated

with IFB-088 and evaluated by behavioural, neurophysiological, morphological and biochemical analyses.

Materials and Methods

All the experiments on *Mpz*R98C/ + knock-in mice, except the myelinating DRG cultures, were performed at the University of Iowa (Iowa City, US), and all the experiments on C3-PMP22 mice were performed at the San Raffaele Scientific Institute (Milan, Italy).

Myelinating DRG Explant Cultures

Dorsal root ganglia (DRG) were dissected from embryos at embryonic day 13.5 (E13.5) and plated singularly on collagen-coated coverslips as previously described [27]. The embryos were genotyped immediately after dissection. Myelination was induced with 50 µg/ml ascorbic acid (Sigma-Aldrich). Treatment with IFB-088 at the indicated concentration was applied for 2 weeks in parallel to the induction of myelination. Samples were then fixed, and rat anti-MBP (1/5) [28] and rabbit anti-NF-H (1/1000, EMD Millipore) primary antibodies were added o/n at 4 °C. The following day, DRGs were washed and FITC- or TRITC-conjugated secondary antibodies (1:200, Cappel) were added for 1 h at room temperature. Specimen were incubated with DAPI (1:1000, SIGMA) and mounted with VECTASHIELD (Vector Laboratories). Eight to 10 images were taken from each DRG using a fluorescence microscope (Leica DM5000) with a 10×objective, and the number of MBP + internodes in each image was counted.

Animal Models

All experiments involving animals were performed in accordance with experimental protocols approved by the San Raffaele Scientific Institute and the University of Iowa Animal Care and Use Committee. *Mpz*S63del transgenic mice [29] and *Mpz*R98C/ + knock-in mice [23] were maintained on the FVB/N background. C3-PMP22 transgenic mice [26] were obtained from the Amsterdam University Medical Center, Amsterdam, the Netherlands. They were maintained on a C57BL/6 J background. C3-PMP22 cohorts for this study were generated via in vitro fertilization following the protocol from the European Mouse Mutant Archive (EMMA)—mouse sperm cryopreservation protocol [30].

Experimental Design

C3-PMP22 Study Starting from post-natal day (PND) 15, mice were administered via oral gavage twice a day (bis in die (*b.i.d.*)). WT mice were administered with vehicle (saline solution: NaCl 0.9%) *b.i.d.*, and C3-PMP22 mice were administered with vehicle *b.i.d.* or IFB-088 0.5 mg/kg *b.i.d.* or 1 mg/kg *b.i.d.* After a 10-week treatment period, mice were tested for treadmill and grip strength. After a 12-week treatment period, mice were analysed for neurophysiology and sacrificed for morphology and biochemistry. Each experiment was performed by a different operator, completely blinded to genotype and treatment.

MpzR98C/ + Study WT and *Mpz*R98C/ + mice were administrated via oral gavage twice a day with vehicle (saline solution: NaCl 0.9%) or IFB-088 1 mg/kg starting from PND30. After 90 days (PND120) and 150 days (PND180) of treatment, mice were tested for rotarod, grip strength and electrophysiology. Animals were then sacrificed for morphology, protein and molecular expression analysis with the evaluator blinded to genotype and treatment.

Treadmill

C3-PMP22 mice were evaluated on treadmills after a 10-week treatment. A grid that delivers a mild electric shock is used to motivate the animal to run. On the first day, mice are trained for 5 min, starting at 6 cm/s; the speed is slowly increased to 10 cm/s. The treadmill has a 5° inclination and delivers a 0.2-mA shock. The following day, measurement is performed: initial speed is set up at 10 cm/s, increased of 2 cm/s every minute. The test ends at exhaustion, when the mouse spends more than 3 s on the electric shock grid. Distance covered, speed and number of shocks were recorded.

Rotarod

*Mpz*R98C/ + mice were evaluated at PND120 and PND180 on an accelerating rotating rod. Mice underwent three training trials on an IITC Life Science Rotarod (Series 8) with a ramp speed from 2 to 20 rpm in 300 s. A 1-h rest was given after each trial, and it was considered valid if the animals ran forward on the rod for at least 10 s. The next day, the latency to fall was recorded three times following the abovementioned protocol for each time point and mouse. The average was used as the outcome value.

Grip Strength

C3-PMP22 Study

The muscular strength was evaluated using a GSM Grip-Strength Meter (Ugo Basile). This test measures the muscular strength using an isometric dynamometer connected to a grid. Once the animal is holding the grid with its forepaws, it is slowly moved backwards pulling the tail, until it

releases the grip. The dynamometer records the maximal force exerted. Each mouse is tested six times.

MpzR98C/ + Study

The strength of all four limbs of WT and *Mpz*R98C/ + mice was evaluated using an automated Grip Strength Meter (Columbus Instruments). Within 1 week after training (10 practice trials using a mesh bar), the peak force exerted by each individual mouse was measured 10 times consecutively with 10-s resting periods and averaged.

Electrophysiological analysis

C3-PMP22 study

The electrophysiological evaluation was performed with a specific EMG system (Neuro-MEP Micro, Neurosoft, Russia), as previously described [31]. Mice were anesthetized with trichloroethanol, 0.02 ml/g of body weight, and placed under a heating lamp to maintain constant body temperature. Sciatic nerve conduction velocity was obtained by stimulating the nerve with steel monopolar needle electrodes. A pair of stimulating electrodes was inserted subcutaneously near the nerve at the ankle. A second pair of electrodes was placed at the sciatic notch to obtain two distinct sites of stimulation, proximal and distal along the nerve. Compound motor action potential (CMAP) was recorded with a pair of needle electrodes; the active electrode was inserted in muscles in the middle of the paw, whereas the reference was placed in the skin between the first and second digits. Sciatic nerve *F*-wave latency measurement was obtained by stimulating the nerve at the ankle and recording the responses in the paw muscle, with the same electrodes employed for the NCV study.

MpzR98C/ + Study

Mice were analysed as above with the following differences. Anaesthesia was with ketamine/xylazine (87.5 mg/kg ketamine, 12.5 mg/kg xylazine). For sensory electrophysiological testing, one pair of loop electrodes were put 0.2 cm and 0.7 cm from the tail base as recording and reference electrodes. A second pair was placed on the tail 3.7 cm (cathode) and 4.2 cm (anode) from the base. A ground electrode was put at the middle of two pairs of loop electrodes. The distal pair was used for stimulation [32].

Morphological Analysis

Mice were sacrificed at the indicated time points, and sciatic and femoral nerves were dissected. Semi-thin section and electron microscope analyses were performed as previously described [33]. The number of amyelinated axons in C3-PMP22 mice was counted blind to genotype and treatment from quadricep femoral nerve semi-thin Sects. (0.5–1 µm thick) stained with toluidine blue, on images taken with a 100 × objective, after whole nerve reconstruction. Similarly, for *Mpz*R98C/ + mice, semithin sections were examined under a 63 × objective. Each consecutive field was captured using a digital camera, and a whole nerve reconstruction was made by using photoshop software. In both studies, *g*-ratio analysis (axonal diameter/fibre diameter) and the size distribution of myelinated fibres (based on axonal diameter) were also measured for all fibres. Four to 8 mice per genotype and condition were analysed. Ultrathin Sects. (90 nm thick) from femoral nerves were cut using an ultracut ultramicrotome, stained with uranyl acetate and lead citrate and examined by transmission electron microscopy (TEM) (Zeiss Leo 912 Omega or JEOL 1230, Peabody, MA).

Protein Extraction and Western Blotting

Mice were sacrificed at the indicated time points, and sciatic nerves were dissected and immediately frozen in liquid nitrogen. Protein extraction was performed as previously described [34, 35]. The following antibodies were used: rabbit anti-Grp78/Bip (1:1000, Novus Biological, NB300-520 or 1:1000, Abcam, ab21685); rabbit anti-Phospho-eIF2α (Ser51) (D9G8) XP™ and eIF2α (D7D3) XP™ (1:2000, Cell Signalling, #3398 and #5324); chicken anti-P0 (PZO, Aves); rabbit anti-PMP22 (AB211052 or AB 861,220; ABCAM); mouse anti-β-tubulin (1:1000, T4026, Sigma); mouse anti-Gapdh (1:1000, Millipore, MAB374); and rabbit anti c-Jun (1:1000, ABCAM, #32,137). Peroxidase-conjugated secondary antibodies (anti-rabbit HRP, DAKO, P0448; anti-chicken IgG-peroxidase, Sigma) were visualized using Amersham ECL or ECL Prime 225 reagent (GE Healthcare) for high-sensitivity chemiluminescent protein detection with UVItec gel analysis systems or using enhanced chemiluminescence (ECL) reagents (Bio-Rad) with autoradiography film (Kodak Scientific Imaging Film, Blue XB). Total proteins were visualized via staining with Coomassie Brilliant Blue R250 staining solution (Bio-Rad). Densitometric quantification was performed with ImageJ.

RNA Isolation and Real-time PCR Analysis

C3-PMP22 Study

Total RNA was extracted using TRIzol (Roche Diagnostic GmbH, Germany), and reverse transcription was performed as described previously [36]. Quantitative RT-PCR

was performed according to the manufacturer's instructions (TaqMan, PE Applied Biosystems Instruments) on an ABI PRISM 7700 sequence detection system (Applied Biosystems Instruments). Normalization was performed using 18S rRNA as reference gene. Target and reference gene PCR amplification was performed in separate tubes with Assay on Demand™ (Applied Biosystems Instruments): 18S assay Hs99999901_s1; Ddit3/Chop, Mm00492097_m1; Xbp-1 s assay, Mm03464496_m1; Hspa5/BiP assay, Mm00517691_m1; ATF4 assay, Mm00515324_m1; Gadd34/PPP1r15a assay, Mm00435119_m1.

MpzR98C/ + Study

Total RNA was extracted using NucleoSpin RNA Plus Kit (740,984.50 Macherey–Nagel GmbH & Co. KG, Germany). Complementary DNA was prepared with SuperScript® III First Strand Synthesis SuperMix (11,752–050, Invitrogen), and samples were analysed as triplicates on a StepOnePlus Real-Time PCR System (Applied Biosystems) detection system using Fast SYBR® Green (4385612, Applied Biosystems). All samples were normalized to Ppia as an endogenous control and expressed relative (threshold cycle (Ct) and $2^{-\Delta\Delta Ct}$) to vehicle sciatic nerve data. The list of primers is shown below:

CHOP forward 5′-CTGCCTTTCACCTTGGAGAC-3′
CHOP reverse 5′-CGTTTCCTGGGGATGAGATA-3′
BiP forward 5′-CATGGTTCTCACTAAAATGAAAGG-3′
BiP reverse 5′-GCTGGTACAGTAACAACTG-3′
Xbp1-s forward 5′-GAGTCCGCAGCAGGTG-3′
Xbp1-s reverse 5′-GTGTCAGAGTCCATGGGA-3′
Ppia forward 5′-AGCACTGGAGAGAAAGGATT-3′
Ppia reverse 5′-ATTATGGCGTGTAAAGTCACCA-3′

IFB-088 Pharmacokinetic Study

Nine males and nine females C57BL/6 J (three animals per sampling time) were treated with a single intraperitoneal administration of IFB-088 at 4 mg/kg. Ten minutes, 30 min, 1 h, 2 h, 4 h, 6 h, and 8 h after administration, animals were briefly anaesthetized with isoflurane and blood was collected. IFB-088 was extracted from plasma samples and measured by liquid chromatography coupled to tandem mass spectrometry (LC–MS/MS) (Eurofins, ADME Bioanalyses).

Statistical Analysis

Group sizes were pre-determined with the G*Power v3.1.9.4 software (Heinrich-Heine-Universität Düsseldorf), to detect differences of at least 1.25 standard deviations between groups, with 80% power an alpha error of 0.05. Data were analysed with GraphPad Prism7.02 software. For behaviour and electrophysiology, outliers have been identified using Grubbs' test and data tested for normality and variance homogeneity. Statistical differences between mean values between two groups were tested using Student's *T*-test or Mann–Whitney. When multiple groups were compared, one-way ANOVA analysis followed by Friedman's, Tukey's, or Dunnett's multiple-comparison test and Kruskal–Wallis analysis followed by Dunn's multiple-comparison test were used, as indicated in the figure legends.

Results

MpzR98C/ + DRG Schwann Cell Co-cultures Show Improved Myelination Following Treatment with IFB-088

Explanted dorsal root ganglia (DRGs) from wild-type (WT) and *Mpz*R98C/ + mice were plated and grown under myelinating conditions [24]. Similar to what was found in explants from *Mpz*Ser63del mice [24], the percentage of myelinated internodes was reduced in explant cultures of *Mpz*R98C/ + mice compared to explants from WT animals (Additional File 1: Supplementary Fig. 1a-b), although higher than in *Mpz*S63del co-cultures. *Mpz*R98C/ + co-cultures were then treated with escalating doses (50, 75, 100 and 125 nM) of IFB-088 and assessed for myelination. The number of myelinated internodes increased with all doses compared to untreated co-cultures with a maximum effect at 100 nM IFB-088 (Fig. 1a, b), similarly to what was observed in *Mpz*S63del explants (Additional File 1: Supplementary Fig. 1c-d and [24]).

IFB-088 Treatment Improves Grip Strength, Rotarod Performance and Nerve Conduction Velocities in MpzR98C/ + Mice

Western blot (WB) on sciatic nerve lysates from 1-month-old *Mpz*R98C/ + mice, which already manifested signs of the disease [23], showed a clear increase of P-eIF2α (Fig. 1c), indicating activation of the PERK pathway of the UPR. We treated 1-month-old WT and *Mpz*R98C/ + mice with either vehicle or 1 mg/kg of IFB-088 twice a day (the dosage shown to be effective in *Mpz*S63del mice) [24] by oral gavage. Throughout the treatment, mice were regularly weighted. As previously reported for *Mpz*S63del mice [24], IFB-088 treatment does not impact body weight (Additional File 1: Supplementary Fig. 2).

After 3 and 5 months of treatment, mice were tested by rotarod, grip strength and neurophysiology. The mice were then sacrificed for morphological and biochemical analyses (Fig. 1d; Additional File 1: Supplementary Fig. 3a). As

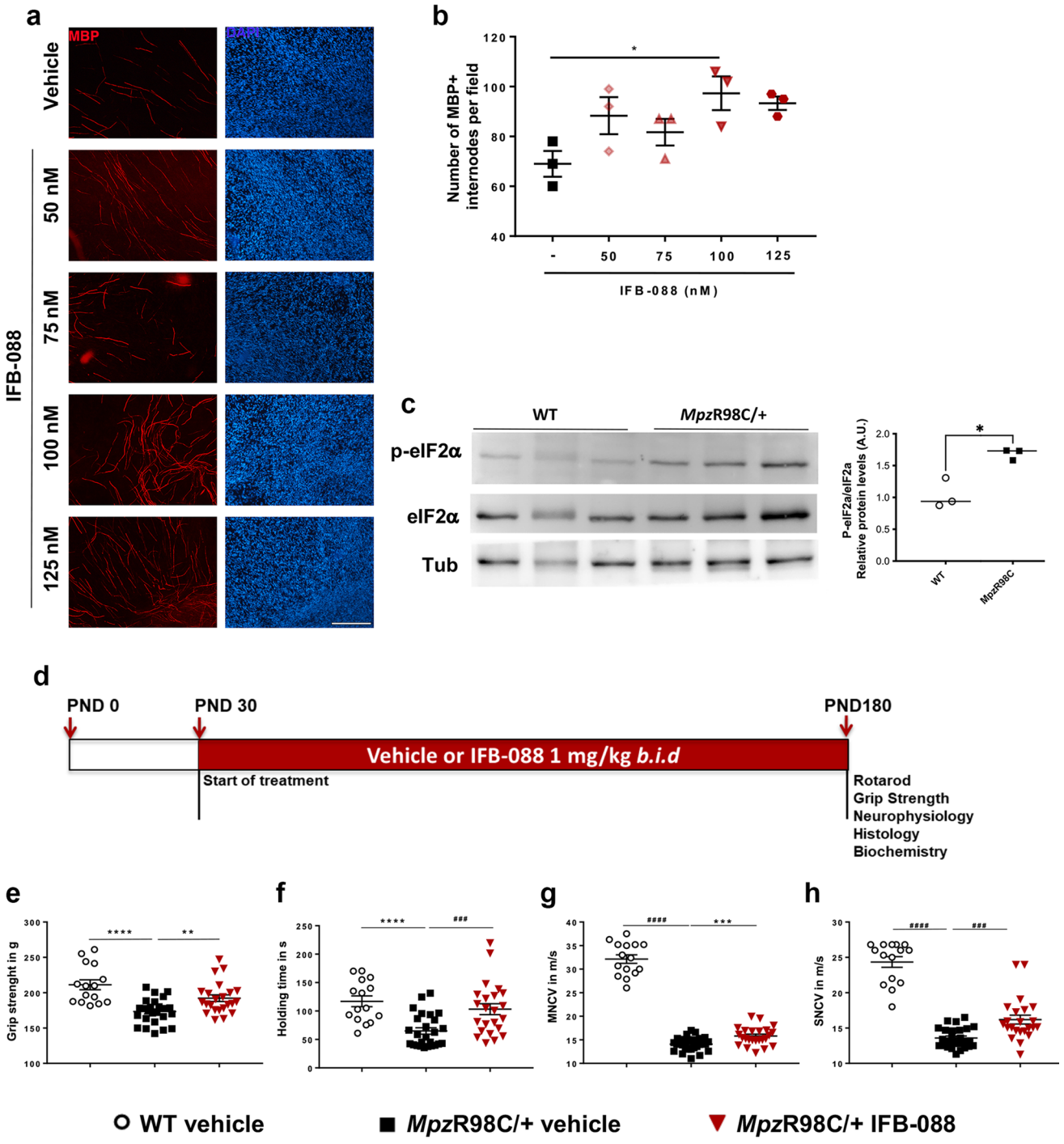

previously observed [24], IFB-088 treatment did not impact WT mouse motor function or neurophysiological parameters (Additional File 1: Supplementary Fig. 3 and Supplementary Fig. 4). *Mpz*R98C/+ mice had reduced grip strength compared to WT animals at PND120 (Additional File 1: Supplementary Fig. 3b) and PND180 (Fig. 1e). After a 5-month treatment, *Mpz*R98C/+ mice showed significant improvement on grip strength compared to vehicle-treated animals (Fig. 1e). Similar improvements were obtained for male and female mice (not shown). We evaluated the mice on the same day for their ability to maintain balance on an accelerating rotarod. We confirmed a significant reduction in the latency to fall in PND120 and PND180 *Mpz*R98C/+ mice as compared to WT mice (Additional File 1: Supplementary Fig. 3c; Fig. 1f) [23, 34]. *Mpz*R98C/+ mice treated with IFB-088 for 5 months, but not 3 months, were able to maintain their balance significantly longer than untreated animals, approaching latencies obtained by WT animals (Fig. 1f; Additional File 1: Supplementary Fig. 3c).

◂**Fig. 1** IFB-088 improves myelination in DRG explants, motor function and nerve conduction velocity from *Mpz*R98C/ + mice. Dorsal root ganglia (DRG) were dissected from embryos (E13.5) of *Mpz*R98C/ + mice. The myelination process was induced with ascorbic acid. After 2 weeks of treatment with vehicle or the indicated concentration of IFB-088, the DRGs were fixed and nuclei visualized by DAPI staining; myelin were visualized by immunostaining with myelin basic protein (MBP) antibody. **a** Representative pictures; scale bar 100 µm. **b** Number of myelinated internodes per field in *Mpz*R98C/ + DRG explant cultures treated with vehicle or the indicated concentration of IFB-088 for 2 weeks. Mean ± SEM; $n = 3$ independent experiments. $^{*}P < 0.05$ one-way ANOVA followed by Friedman's test. **c** Representative western blot (WB) for P-eIF2α, total eIF2α and tubulin on sciatic nerve protein extracts from 1-month-old WT and *Mpz*R98C/ + mice. The graph shows the densitometric quantification of the P-eIF2α/eIF2α ratio; $^{*}P < 0.05$ by unpaired *t*-test. **d** Diagram of the treatment strategy. Thirty-day-old WT and *Mpz*R98C/ + mice were orally administered with vehicle or IFB-088 1 mg/kg *b.i.d.* for 5 months. **e** Four limb grip strength max values average of 10 trials. Data were expressed in grams (g) as mean ± SEM; $n = 15$–26 mice per condition. (**f**) Rotarod analysis. Data are expressed in seconds (s) as mean ± SEM; $n = 15$–26 mice per condition. **g** Motor nerve conduction velocity (MNCV). Data are expressed in meters/second (m/s) as mean ± SEM; $n = 15$–27 mice per condition. **h** Sensory nerve conduction velocity (SNCV). Data are expressed in meters/second (m/s) as mean ± SEM. $n = 15$–26 mice per condition. $^{**}P < 0.01$; $^{***}P < 0.001$, $^{****}P < 0.0001$ by Student's *t*-test; $^{\#\#\#}P < 0.001$, $^{\#\#\#\#}P < 0.0001$ by Mann–Whitney

Neurophysiological testing confirmed marked slowing in motor nerve conduction velocity (MNCV) and sensory nerve conduction velocity (SNCV) in *Mpz*R98C/ + mice at PND120 (Additional File 1: Supplementary Fig. 3d-e) and PND180 (Fig. 1g, h) [23, 34]. No significant differences in compound muscle action potential (CMAP) and sensory nerve action potential (SNAP) amplitudes were observed between WT and *Mpz*R98C/ + mice (not shown). A 5-month treatment with IFB-088 significantly improved both MNCV and SNCV of *Mpz*R98C/ + mice (Fig. 1g, h). The positive impact of IFB-088 treatment on *Mpz*R98C/ + SNCV was also observed after 3 months of treatment (Additional File 1: Supplementary Fig. 3e).

IFB-088 Treatment Improves Nerve Morphology, Partially Reduces ER Stress and Corrects the Expression of Schwann Cell Differentiation Marker in MpzR98C/ + Mice

On morphometric analysis, nerves from *Mpz*R98C/ + mice demonstrated marked abnormal myelin as attested by reduced myelin thickness and increased *g*-ratio (Fig. 2). After a 5-month IFB-088 treatment, quadriceps femoral nerves from *Mpz*R98C/ + mice showed reduced the *g*-ratio (ratio between axon diameter and axon + myelin diameter) (Fig. 2a–c) and increased myelin thickness (Fig. 2d–f and data not shown). Compared to vehicle-treated nerves. Detailed ultrastructural analysis performed via EM confirmed the thin myelin sheath surrounding *Mpz*R98C/ + axons, which looks thicker after IFB-088 treatment (Fig. 2g), with apparently normal compaction and periodicity (Fig. 2g, insets).

We previously showed that *Mpz*R98C/ + mice have increased expression of ER-chaperone immunoglobulin heavy chain-binding protein (BiP) and glucose-regulated protein 94 (Grp94), as part of an ER-stress response. We also demonstrated an altered phenotype of myelinating Schwann cells in which the expression of c-Jun, a transcription factor that inhibits myelination [37], was increased [23]. Therefore, we investigated the expression of mRNA (Fig. 3a–c) and protein levels (Fig. 3d–f) in a variety of genes known to play a role in these processes. As previously described, *Mpz*R98C/ + mice presented an increase in the expression of ER stress and UPR markers *BiP*, C/EBP homologous protein (*Chop*) and spliced X-box-binding protein-1 (*Xbp1s*) and a higher level of the negative regulator of myelination c-Jun compared to WT mice (Fig. 3). IFB-088 treatment, which as expected resulted in an increase in eIF2alpha phosphorylation levels (Fig. 3d, e), led to a reduction in the levels of *Chop* and *BiP* mRNA (Fig. 3a, b) and BiP protein (which however did not reach statistical significance) (Fig. 3d, f), whereas the levels of *Xbp1s* were unchanged (Fig. 3c). Finally, c-Jun protein levels were significantly reduced by IFB-088 (Fig. 3d, g). Altogether our data suggest that treatment with IFB-088 partially reduced stress levels in *Mpz*R98C/ + nerves and lifted c-Jun inhibition, allowing myelination to proceed.

Nerves from the CMT1A Mouse Model C3-PMPP22 Show Alteration of Myelin Protein Stoichiometry and Activation of ER-Stress Pathways

To address whether IFB-088 could be a viable treatment also for CMT1A, we took advantage of the C3-PMP22 mouse (supposed to carry 3–4 extra copies of PMP22) [26]. WB performed for protein extraction from C3-PMP22 nerves at 4 months demonstrated a reduced expression of P0 (MPZ), the most abundant myelin protein, but similar PMP22 levels to WT nerves. As a result, there was a relative overexpression of PMP22 protein in C3-PMP22 nerves (Fig. 4a).

To test whether the excess of PMP22 would lead to proteostatic stress, we measured the mRNA levels for a subset of well-known UPR markers. This revealed a small increase in the expression of the general ER-stress marker *BiP* (downstream of the ATF6 arm of the UPR), and a significant upregulation of *Chop* and of the protein phosphatase 1 regulatory subunit 15A (*Gadd34/Ppp1r15a*), two downstream targets of the PERK/P-eIF2α pathway, whereas *Xbp1s*, a target of the inositol requiring enzyme 1 (IRE1) arm, and the activating transcription factor 4 (*Atf4*) were not increased (Fig. 4b). WB for BiP and P-eIF2α confirmed the activation of stress pathways in these nerves (Fig. 4c, d). These results

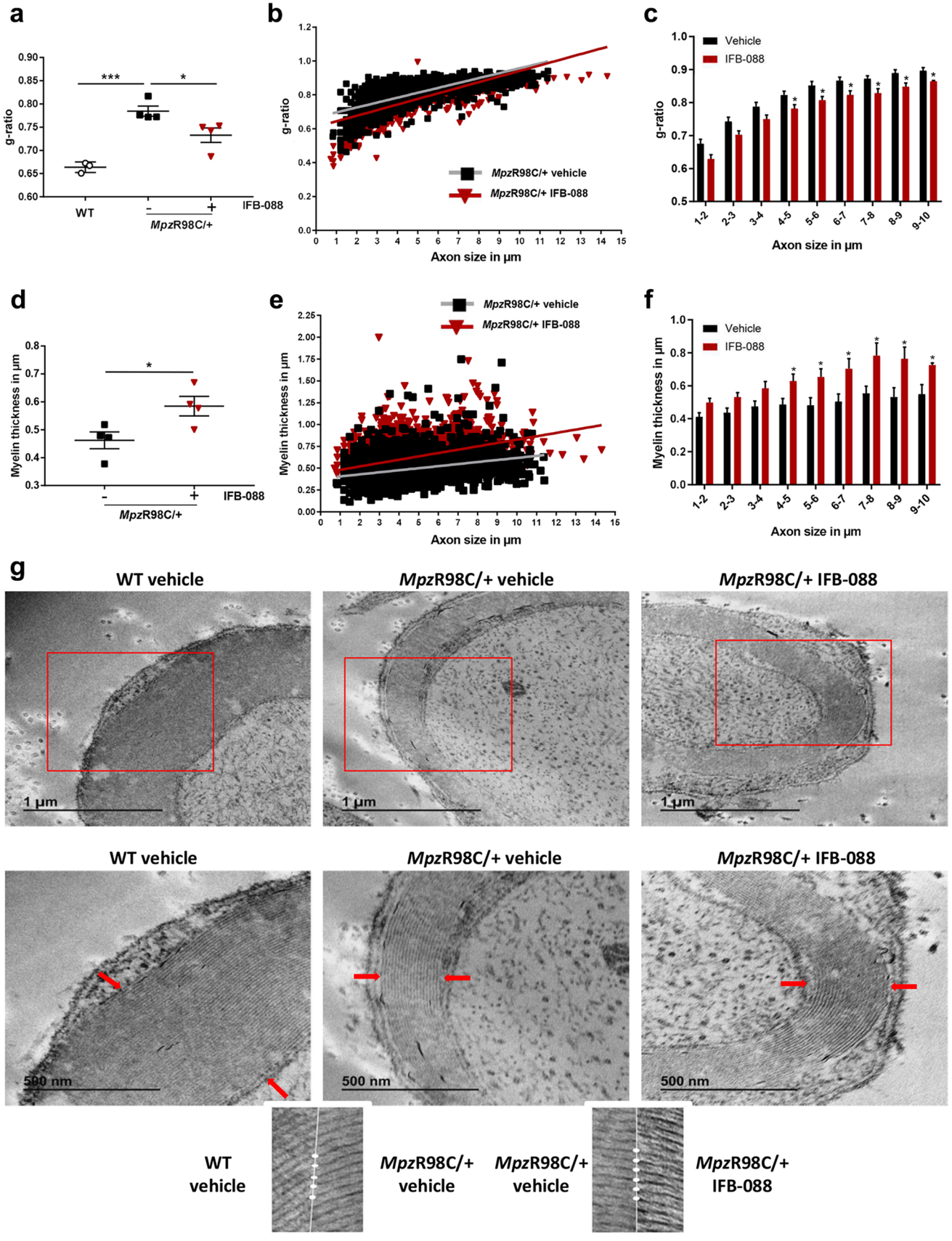
a
g-ratio
***
*
WT
MpzR98C/+
IFB-088
b
g-ratio
MpzR98C/+ vehicle
MpzR98C/+ IFB-088
Axon size in µm
c
Vehicle
IFB-088
g-ratio
Axon size in µm
d
Myelin thickness in µm
IFB-088
MpzR98C/+
e
MpzR98C/+ vehicle
MpzR98C/+ IFB-088
Myelin thickness in µm
Axon size in µm
f
Vehicle
IFB-088
Myelin thickness in µm
Axon size in µm
g
WT vehicle
MpzR98C/+ vehicle
MpzR98C/+ IFB-088
1 µm
500 nm
WT vehicle
MpzR98C/+ vehicle
MpzR98C/+ vehicle
MpzR98C/+ IFB-088

◂**Fig. 2** IFB-088 treatment improves *Mpz*R98C/ + mice quadriceps femoral nerve morphology. **a** *g*-ratios performed on toluidine blue–stained semi-thin sections of quadriceps femoral nerve from *Mpz*R98C/ + mice treated with vehicle *b.i.d.* or IFB-088 1 mg/kg *b.i.d.* for 5 months. Data are expressed as mean ± SEM. $n = 4$ mice per condition. $^*P < 0.05$ by Student's *t*-test. **b** Scatter plot of quadriceps femoral nerve *g*-ratios toward the axon diameter from *Mpz*R98C/ + mice treated with vehicle *b.i.d.* or IFB-088 1 mg/kg *b.i.d.* $n = 4$ mice per condition. **c** Average g-ratio plotted by axon diameter. $^*P < 0.05$ by Student's *t*-test. **d** Myelin thickness measured from toluidine blue–stained semi-thin sections of quadriceps femoral nerve from *Mpz*R98C/ + mice treated with vehicle *b.i.d.* or IFB-088 1 mg/kg *b.i.d.* for 5 months. Data are expressed in µm as mean ± SEM. $n = 4$ mice per condition. $^*P < 0.05$ by Student's *t*-test. **e** Scatter plot of quadriceps femoral nerve myelin thickness toward axon diameter from *Mpz*R98C/ + mice treated with vehicle *b.i.d.* or IFB-088 1 mg/kg *b.i.d.* $n = 4$ mice per condition. **f** Average myelin thickness plotted by axon diameter. $^*P < 0.05$ by Student's *t*-test. **g** Ultrathin electron microscopy sections of quadriceps femoral nerve from WT mice treated with vehicle *b.i.d.* and from *Mpz*R98C/ + mice treated with vehicle *b.i.d.* or IFB-088 1 mg/kg *b.i.d.* for 5 months. Lower panels are higher magnification images of upper panels. Scale bar 1 µm for top panels, and 500 nm for bottom panels. The insets show normal myelin compaction and periodicity

showed that C3-PMP22 mice present an alteration of myelin protein stoichiometry associated with the activation of ER-stress pathways.

IFB-088 Treatment Improves Motor Capacity and MNCV in CMT1A Mice

We treated C3-PMP22 mice with either 0.5 mg/kg or with 1 mg/kg of IFB-088 twice a day by oral gavage. The treatment started at PND15, when the disease is already manifested as shown by severe myelination defects, altered myelin protein stoichiometry and activation of ER-stress pathways (Additional File 1: Supplementary Fig. 5).

After 10 weeks of treatment, C3-PMP22 mice were tested for motor capacity and, after 12 weeks of treatment, for neurophysiology. They were then sacrificed for morphological and biochemical analyses (Fig. 5a). Treadmill analysis showed that C3-PMP22 mice were severely impaired compared to WT mice (Fig. 5b). IFB-088 treatment at 1 mg/kg *b.i.d.* showed a small but significant improvement as compared to vehicle-treated mice (Fig. 5b). However, the operator (blind to treatment) noticed that all C3-PMP22 male mice ran very poorly. Therefore, the mice were stratified by gender. C3-PMP22 female mice treated with IFB-088 1 mg/kg *b.i.d.* had a significant amelioration in motor capacity, which increased twofold compared to vehicle-treated mice (Fig. 5c). Male mice also had a comparable twofold improvement with the same dosage, but the baseline was very poor (Fig. 5d).

Grip strength confirmed that C3-PMP22 mice were impaired compared to WT mice. IFB-088 treatment did not improve strength when the mice were analysed altogether (Fig. 5e). However, when divided by gender, C3-PMP22 male mice showed a trend towards improvement at 0.5 mg/kg *b.i.d.* which became significant for the 1-mg/kg *b.i.d.* of IFB-088 (Fig. 5g). This positive impact was not seen in C3-PMP22 female mice (Fig. 5f).

Finally, we assessed a series of neurophysiological parameters (MNCV, F-wave latency, CMAP) which revealed a severe impairment in C3-PMP22 mice as compared to WT controls (Fig. 5h and not shown), as previously reported [26]. Treatment with both 0.5 and 1 mg/kg *b.i.d.* IFB-088 showed a modest improvement in MNCV after a 12-week treatment, which reached significance for the 0.5-mg/kg *b.i.d.* dose (Fig. 5h). Stratification per gender revealed that the improvement was restricted to female mice, for which the amelioration was statistically significant at both dosages (Fig. 5i). Only IFB-088-treated C3-PMP22 female mice displayed MNCV over 20 m/s. On the contrary, in C3-PMP22 male mice there was no improvement, and actually the 1-mg/kg *b.i.d.* dose showed a small worsening that, although marginal, reached statistical significance (Fig. 5j). None of the other neurophysiological parameters measured were improved by the treatment (not shown).

IFB-088 Treatment Improves Nerve Morphology, Reduces ER-Stress Level, and Partially Readjusts Myelin Protein Stoichiometry in CMT1A Mice

Previous analysis suggested that C3-PMP22 mouse motor nerves were more affected than sensory nerves [26, 38]. Therefore, we dissected quadriceps femoral nerve, predominantly motor nerve and sciatic nerve which is a mixed nerve with many sensory axons. Transverse sections of sciatic nerves showed an increase in the myelination of large-calibre fibres in mice treated with IFB-088. In both male and female C3-PMP22 nerves, large-calibre axons were almost invariably amyelinated (where by amyelinated we refer to any axon with diameter > 1 µm, which is in contact with a Schwann cell but not myelinated by it). After IFB-088 treatment, many of the large axons were myelinated (Additional File 1: Supplementary Fig. 6). Similarly, in untreated femoral nerves most large-calibre axons were amyelinated whereas small calibre axons tended to be hypermyelinated (Fig. 6a, b). As in sciatic nerves, treatment with IFB-088 partially corrected these abnormalities with myelin wrapping appearing around large axons at both 0.5 and 1 mg/kg *b.i.d.* of IFB-088 (Fig. 6a, b). No gross differences were detected between female and male nerves (Fig. 6a, b; Additional File 1: Supplementary Fig. 6).

Cross sections of the entire femoral nerve from 2 to 4 mice per condition for both genders were reconstructed and, for each nerve, the entire number of myelinated or amyelinated axons was counted (Table 1).

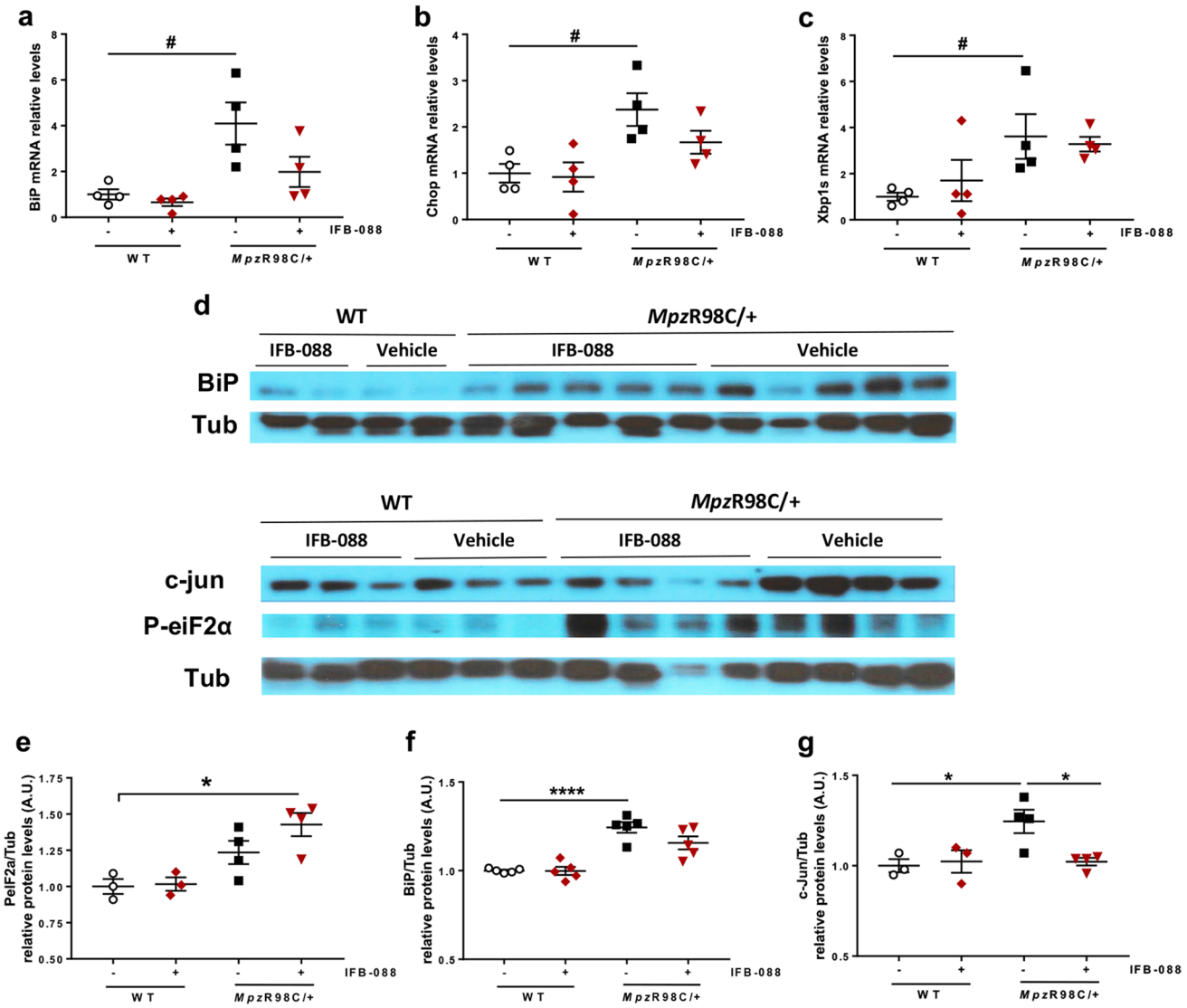

Fig. 3 IFB-088 treatment reduces ER stress and Schwann cell differentiation marker expression in *Mpz*R98C/+ sciatic nerve. Evaluation of mRNA (**a–c**) and protein levels (**d–f**) on sciatic nerve samples from WT and *Mpz*R98C/+ mice treated with vehicle *b.i.d.* or IFB-088 1 mg/kg *b.i.d.* for 5 months. mRNA relative levels of *Bip* (**a**), *Chop* (**b**) and *Xbp1s* (**c**) determined by qRT-PCR. $n=4$ per condition. #$P<0.05$ by Mann–Whitney. **d** Western blot images for BiP, P-eIF2α, and c-Jun. Quantification relative to tubulin for P-IeF2α (**e**), BiP (**f**) and c-Jun (**g**), $n=3$–5 per condition. *$P<0.05$, **$P<0.01$ by Student's *t*-test

This analysis identified 27.2 ± 2.4% amyelinated large axons in C3-PMP22 vehicle–treated nerves. Treatment with IFB-088 0.5 or 1 mg/kg *b.i.d.* reduced the percentages to 19.9 ± 1.3% and 21.9 ± 1.4%, representing a 27% and 20% improvement respectively. The number of amyelinated axons was slightly greater for females (29.9 ± 1%) than for males (25.4 ± 3.9%) which also showed more variability. In males, the treatment with IFB-088 0.5 or 1 mg/kg *b.i.d.* had a similar effect, reducing amyelinated axons by roughly 20%, whereas in females the IFB-088 0.5-mg/kg *b.i.d.* treatment reduced amyelinated axons by 34%, while the IFB-088 1-mg/kg *b.i.d.* treatment reduced it by 20% (Table 1).

Analysis of myelin thickness by *g*-ratio showed a remarkable difference in the scatter plot between WT and C3-PMP22 mice. The slope for C3-PMP22 mice was much steeper, mostly due to the large group of hypermyelinated small axons (diameter < 1 µm) accompanied by the almost complete absence of myelination in axons larger than 5 µm (Fig. 6c). Indeed, whereas there were no myelinated axons smaller than 1 µm in WT nerves, 4.4% of the axons myelinated in quadriceps femoral nerves from C3-PMP22 mice had a diameter lower than 1 µm, indicating an aberrant hypermyelinating phenotype. Conversely, 45.9% of myelinated axons in nerves from WT mice had a diameter larger than 5 µm, a percentage that was reduced to only 3.9% of

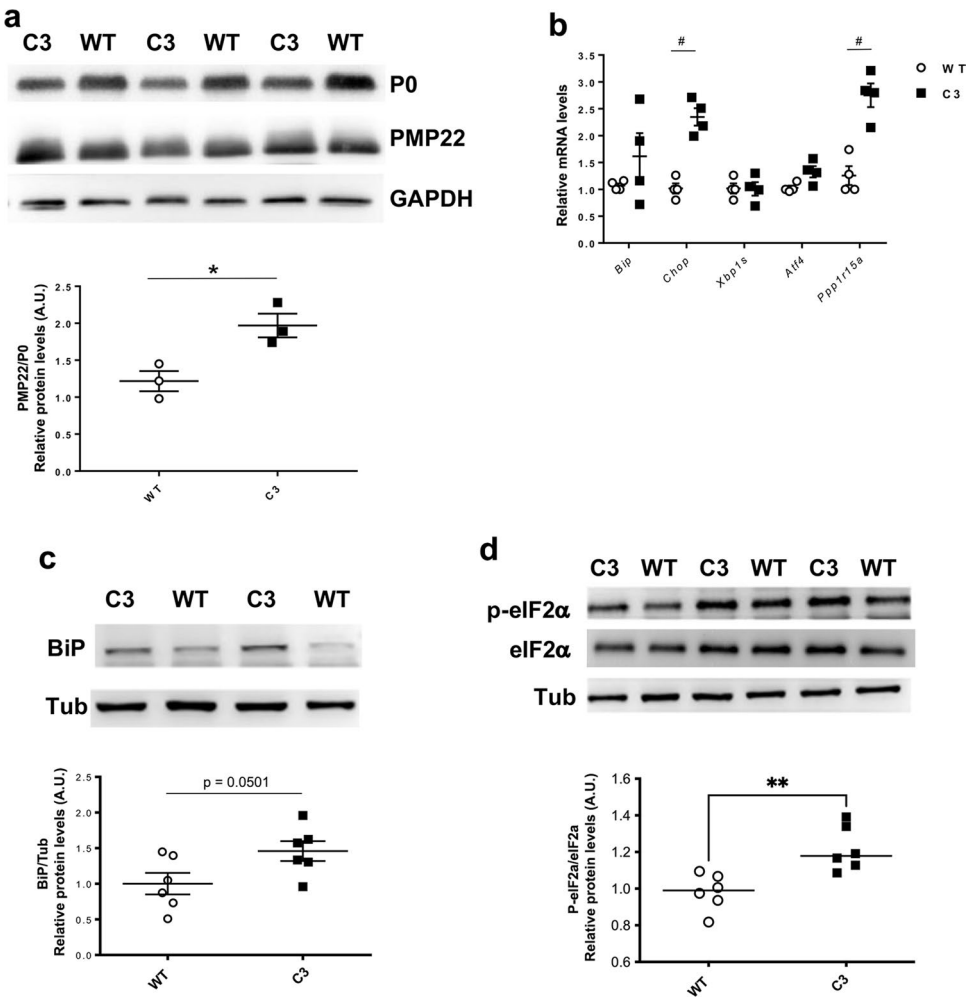

Fig. 4 C3-PMP22 mice show a relative overexpression of PMP22 associated with the expression of ER stress/UPR markers. **a** Evaluation of PMP22, P0 and GAPDH protein levels by WB in sciatic nerve protein lysates from 4-month-old WT and C3-PMP22 (C3) mice. Top: representative picture. Bottom: quantification of the PMP22/P0 protein ratio; $n=3$ per condition. $^{*}P<0.05$ by Student's *t*-test. **b** Evaluation of *Bip*, *Chop*, *Xbp1s*, *Atf4* and *Gadd34/Ppp1r15a* mRNA levels by qRT-PCR on sciatic nerve samples from 4-month-old WT and C3-PMP22 (C3) mice; $n=4$ per condition. $^{\#}P<0.05$ Mann–Whitney. **c** Evaluation of BiP and tubulin protein levels by WB in sciatic nerve protein lysates from 4-month-old WT and C3-PMP22 (C3) mice. Top: Representative picture. Bottom: quantification relative to tubulin; $n=6$ per condition. Student's *t*-test. **d** Evaluation of P-eIF2α, total eIF2α and tubulin protein level by WB in sciatic nerve protein lysates from 1-month-old WT and C3-PMP22 (C3) mice. Top: representative picture. Bottom: quantification of the P-eiF2α level relative to total eIF2α; $n=6$ per condition. $^{**}P<0.01$ by unpaired *t*-test

the myelinated axons in C3-PMP22 mice (Fig. 6d). IFB-088 treatment partially corrected these abnormalities. The percentage of myelinated axons smaller than 1 µm was reduced to 2.1% and 2.3% by the IFB-088 0.5-mg/kg *b.i.d.* and 1-mg/kg *b.i.d.* treatments respectively, whereas the percentage of myelinated axons with a diameter larger than 5 µm rose to 12.4% and 8.5%, respectively (Fig. 6d). Stratification of male and female mice showed that the amelioration in the hypermyelinating phenotype in small-calibre axons was exclusively present in females, as visible in the scatterplots (Additional File 1: Supplementary Fig. 7a-b), even though the overall *g*-ratio in vehicle-treated C3-PMP22 males and females was virtually identical (0.61 ± 0.013 in males vs 0.61 ± 0.015 in females). In both C3-PMP22 males and females, IFB-088 treatment increases the number of myelinated axons with diameter larger than 5 µm (Additional File 1: Supplementary Fig. 7c-d).

Detailed analysis by transmission electron microscopy (TEM) on transverse sections from quadriceps femoral nerves confirmed that in C3-PMP22 nerves, small diameter axons (even smaller than 1 µm) were surrounded by an abnormally thick myelin sheath. In female nerves, treatment with IFB-088 almost completely corrected this phenotype (Fig. 6e; Additional File 1: Supplementary Fig. 7a). At the same time, large-calibre axons were either not myelinated or presented a very thin layer of myelin (probably

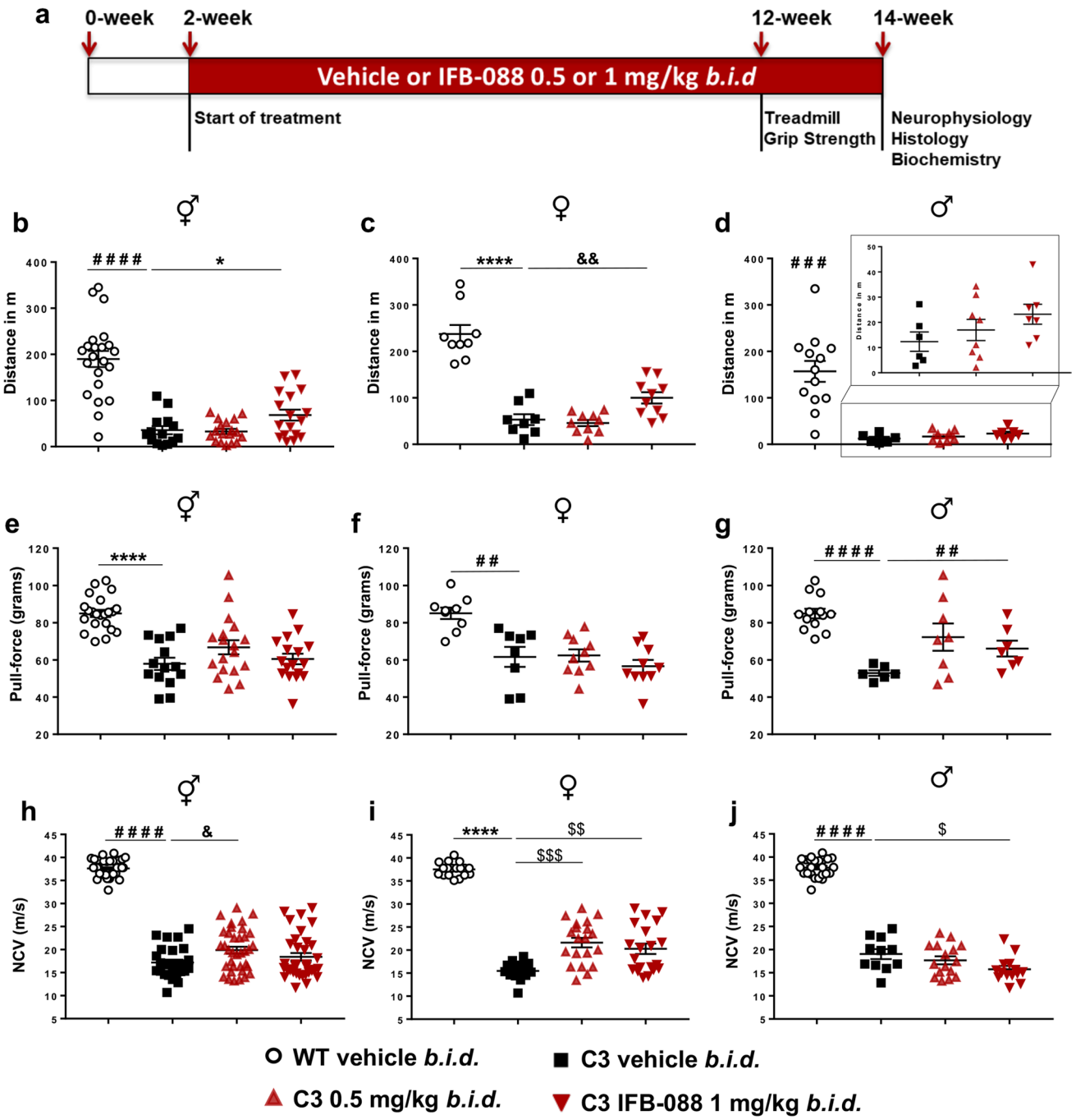

Fig. 5 IFB-088 treatment improves motor function and nerve conduction velocity in C3-PMP22 mice. **a** Diagram of the treatment strategy. Fifteen-day-old WT and C3-PMP22 (C3) mice were orally administered with vehicle *b.i.d.* or IFB-088 at 0.5 or 1 mg/kg *b.i.d.* for 12 weeks. **b** Treadmill analysis performed after 10-week of treatment. Data from males and females expressed in meter (m) as mean ± SEM; $n = 14–22$ mice per condition. **c** Data from females; $n = 8–10$ mice per condition. **d** Data from males, $n = 6–13$ mice per condition. **e** Forepaws grip strength average of 6 trials performed after 10 weeks of treatment. Data were expressed in pull force (grams) as mean ± SEM. $n = 14–22$ mice per condition. **f** Data from females; $n = 8–10$ mice per condition. **g** Data from males, $n = 6–13$ mice per condition. **h** Motor nerve conduction velocity (MNCV) performed after 12 weeks of treatment. Data from males and females expressed in meters/second (m/s) as mean ± SEM. $n = 14–21$ mice per condition. (**i**) Data from females, $n = 8–10$ mice per condition. (**j**) Data from males, $n = 6–12$ mice per condition. $^{*}P < 0.05$; $^{**}P < 0.01$; $^{****}P < 0.0001$ by Student's *t*-test. $^{\#}P < 0.05$; $^{\#\#\#}P < 0.001$; $^{\#\#\#\#}P < 0.0001$ by Mann–Whitney. $^{\&}P < 0.05$; $^{\&\&}P < 0.01$ by one-way ANOVA followed by Dunnett's test. $^{\$}P < 0.05$; $^{\$\$}P < 0.01$; $^{\$\$\$}P < 0.001$ by Kruskal–Wallis followed by Dunn's test

corresponding to 2–3 wraps of Schwann cell membrane). Treatment with IFB-088 allowed myelination to proceed also in large-calibre fibres (Fig. 6f). Importantly, this newly formed myelin appeared to have a proper structure and compaction/periodicity.

As previously shown, C3-PMP22 nerves presented an increased expression of the ER-stress marker BiP and an unbalance between PMP22 and P0 protein levels. We therefore wanted to test whether IFB-088 treatment could correct these features. WB analysis showed that treatment with both dosages of IFB-088 normalized BiP expression to WT levels (Fig. 7a, b), and that there was a partial (although not complete) readjustment of the PMP22/P0 protein ratio (Fig. 7a, c), suggesting an overall improvement in nerve proteostasis.

Discussion

The maintenance of correct protein homeostasis (proteostasis) is tightly controlled by protein quality control (PQC) mechanisms [8]. Myelinating Schwann cells, which need to synthesize large amounts of lipids and proteins, are particularly susceptible to failures in PQC. Alterations in proteostasis, deficits in PQC and the activation of ER-stress/UPR have been implicated in several myelin disorders [39]. Here we show that the small-molecule IFB-088 is able to readjust protein homeostasis and to ameliorate disease features in two models of demyelinating CMT1, the *Mpz*R98C/ + (CMT1B) and the C3-PMP22 (CMT1A) mice.

IFB-088 Improves Disease Features in CMT1B Mice

We demonstrated that IFB-088 effectively mitigates the peripheral neuropathy in *Mpz*R98C/ + mice, using in vitro as well as in vivo studies. In vitro, IFB-088 enhanced myelination in *Mpz*R98C/ + DRGs explant co-cultures. In vivo, 5-month IFB-088 treatment improved motor performance, nerve conduction velocity and peripheral nerve morphology of *Mpz*R98C/ + mice. Our prior studies demonstrated that ER chaperones such as BiP and the transcription factor CHOP are upregulated in *Mpz*R98C/ + mice consistent with their ER-stress response. We also previously demonstrated that the transcription factor c-Jun, which inhibits PNS myelination [37], was upregulated in *Mpz*R98C/ + mice [23]. We now show that treatment with IFB-088 reduced ER-stress and decreased the expression of the negative regulator of myelination c-Jun.

IFB-088 treatment effects, while significant in *Mpz*R98C/ + mice, were less pronounced than those observed in *Mpz*Ser63del animals [24]. Morphological as well as molecular deficits were often prevented in the *Mpz*Ser63del mice [24] but only showed improvement in the *Mpz*R98C/ + . We posit several reasons for these differences. First, *Mpz*R98C/ + mice may be considered a "more authentic disease model" than the *Mpz*Ser63del animals, and this may contribute to the different responses to treatment between the two models. The *Mpz*R98C/ + mice have had the mutation "knocked in" to the endogenous mouse *Mpz* allele [23]. Alternatively, the *Mpz*Ser63del mice are transgenic animals and still retain two WT *Mpz* alleles in addition to the *Mpz*Ser63del-expressing transgene [29]. Thus, *Mpz*Ser63del mice have two copies of WT *Mpz* as opposed to the one in *Mpz*R98C/ + mice to generate the normal protein. Secondly, the R98C *MPZ* neuropathy in humans is more severe than that caused by Ser63del *MPZ*. Patients with R98C *MPZ* (also called R69C by an earlier numbering system) have a dysmyelinating neuropathy and present with delayed developmental milestones, often not walking independently until after 2 years of age. Affected patients may require walkers or wheelchairs for ambulation prior to reaching adulthood, and typically have MNCV < 10 m/s [18, 40]. Patients with the Ser63del *MPZ* mutation typically reach developmental milestones on time, walk independently by a year of age and only slowly develop symptoms over the first two decades of life. They have not required more than ankle foot orthotics to ambulate even in adulthood [41]. In humans, *MPZ*S-63del MNCV are in the 20–30-m/s range, similar to what is observed in patients with CMT1A [41]. Thus, clinically, the Ser63del *MPZ* mutation is considered to be a demyelinating rather than dysmyelinating neuropathy. Taken together, these data suggest that the *Mpz*R98C mouse model causes a more severe neuropathy, which would be expected to be more difficult to reverse than the neuropathy caused by the Ser63del *Mpz* mutation.

How alleviating ER-stress improves the neuropathy caused by the R98C and Ser63del *MPZ* mutations remains an important issue. It is unlikely that augmenting UPR activity improves myelination by allowing R98C P0 to be transported to and inserted into PNS myelin. Introducing a cysteine into the P0 extracellular domain at codon 98 would be predicted to disrupt the disulphide bridge between existing cysteines at codons 50 and 127 [42]. This would in turn disrupt the secondary and tertiary structures of the extracellular domain that are necessary to create P0 tetramers in cis and trans to compact myelin [42], as already elegantly shown for the *Mpz*S63C mutation [29, 43]. We believe it more likely that treatment benefits from IFB-088 occur by facilitating the Schwann cell ability to degrade the R98C P0 as well as transport WT P0 to myelin. Myelinating Schwann cells generate very large amounts of proteins and lipids to form and maintain the myelin sheath [44, 45]. Processing and properly folding P0 glycoprotein in the ER are particularly demanding as P0 is, by far, the major PNS myelin protein, comprising approximately 50% of all PNS myelin proteins [46] and 2% of all Schwann cell transcripts during the

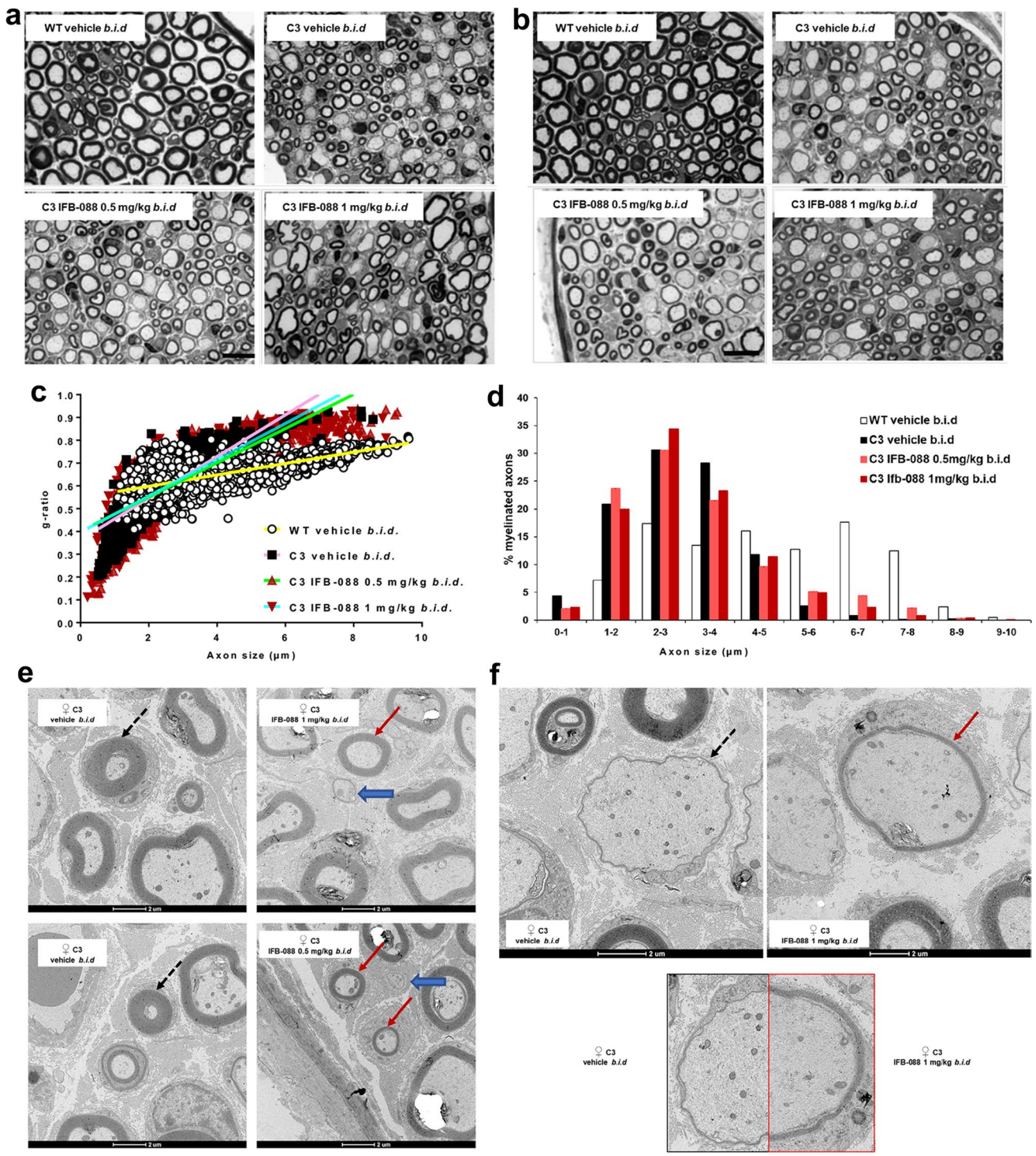

peak of myelination [47]. Folding and post-translationally processing P0 by ERQC pathways are a major undertaking for the ER, even when the protein is in its WT form [48]. The task is increased when a mutation such as R98C makes folding the protein more difficult. Schwann cells typically target misfolded proteins for degradation, through ubiquitination and proteasomal processing. Both protein degradation and proteosome function have been shown to be impaired in *Mpz*Ser63del mice [49, 50], and this is likely to be the case with *Mpz*R98C/+ mice as well. We predict that IFB-088-mediated translational attenuation through persistent phosphorylation of eIF2α will better enable Schwann cells to target R98C P0 for degradation, readjusting protein homeostasis as shown in *Mpz*Ser63del mice [24, 28]. In support

◂**Fig. 6** IFB-088 treatment improves C3-PMP22 mice quadriceps femoral nerve morphology. Toluidine blue–stained semithin sections of quadriceps femoral nerve from **a** female and **b** male WT mice treated with vehicle *b.i.d.* and C3-PMP22 (C3) mice treated with vehicle *b.i.d.* or IFB-088 at 0.5 or 1 mg/kg *b.i.d.* for 12 weeks. Scale bar, 10 µm; *g*-ratio measurement has been performed on toluidine blue–stained semi-thin sections. **c** Scatter plot of quadriceps femoral nerve *g*-ratios from WT mice treated with vehicle *b.i.d.* and C3-PMP22 (C3) mice treated with vehicle *b.i.d.* or IFB-088 at 0.5 or 1 mg/kg *b.i.d*. Note the "cloud" of axons with diameter lower than 1 µm present only in C3-PMP22 nerves (untreated and treated) and the considerable increase in the number of myelinated axons larger than 5–6 µm in IFB-088-treated C3-PMP22 nerves. $n = 5$–8 nerves per condition. **d** Percentage of myelinated axons per axons size; $n = 5$–8 nerves per condition. **e**, **f** TEM analysis of quadriceps femoral nerve from C3-PMP22 (C3) mice treated with vehicle *b.i.d.* or IFB-088 at 1 mg/kg *b.i.d.* **e** In C3-PMP22 vehicle–treated nerves, small-calibre axons are abnormally hypermyelinated (black dotted arrows). Treatment with IFB-088 results in normal-looking myelin in axons larger than 1 µm (red arrows) or in almost no myelin in smaller axons (blue larges arrows). **f** In C3-PMP22 vehicle–treated nerves, large-calibre axons are basically amyelinated or with only a very thin layer of myelin (left panel). After treatment with IFB-088 (right panel), a subgroup of large-calibre axons showed a properly compacted (albeit still rather thin) myelin sheath. A side-by-side comparison of myelination in two axons with similar calibre is shown in the lower panel

of this hypothesis, it has been recently shown that promoting degradation by stimulating the proteasome ameliorates proteostasis and improves the phenotype of *Mpz*Ser63del mice [51]. We have previously shown that UPR activation causes *Mpz*R98C and *Mpz*S63del Schwann cells to enter a limited differentiation state in part by upregulating C-Jun expression; c-Jun, a transcription factor, negatively regulates myelination [37, 52]. As a result of this inhibition, myelin protein expression, including P0, decreases so that there is less mutant P0 for the ER to process [23]. IFB-088 treatment reduces the expression of the UPR marker BiP in *Mpz*R98C/ + mice, suggesting a reduction in ER stress upon treatment. In addition, IFB-088 treatment decreases c-Jun expression and increases peripheral nerve myelination suggesting that inhibition of myelination is lifted. Restoring the Schwann cell phenotype will enable more WT P0 from the normal allele to reach myelin and contribute to clinical improvement. Supporting this explanation is the fact that we have recently demonstrated that patients who are haploinsufficient of *MPZ* have only a mild, late-onset neuropathy, much milder than the neuropathy caused by R98C or Ser63del *MPZ* mutations [53].

C3-PMP22 Mice Show Altered Proteostasis

The overexpression of PMP22 in animal models is sufficient to cause neuropathy, suggesting that increased dosage of PMP22 is the main contributing factor in CMT1A pathology [54, 55]. How the extra copy of *PMP22*-caused diseases is not fully understood, but studies in rodent models as well as in CMT1A patient–derived fibroblast show that PMP22 can form cytosolic aggregates accompanied by reduced proteasomal activity, which may ultimately lead to cytotoxicity [9–11]. PMP22 is a highly metastable protein, with more than 80% of newly synthesized PMP22 rapidly degraded by the proteasome, via ER-associated degradation (ERAD) [7, 56]. Recent in vitro work suggested that in normal conditions, the levels of expression of PMP22 are close to the saturation capacity of the ERQC systems, and that overexpression of PMP22 leads to a disproportionate increase in misfolding and mis-trafficking [57]. Accordingly, examination of sciatic nerves from C22 mice, which show a severe dysmyelinating neuropathy, revealed increased expression of UPR markers such as BiP and CHOP [15]. In human, levels of PMP22 protein in CMT1A patient skin biopsies are elevated, even though the levels are more variable than in non-CMT1A samples [58, 59]. High levels of PMP22 protein have also been reported in sural nerve biopsies from CMT1A patients [60, 61]. Although the exact mechanism underlying the pathogenicity associated with expression of a third copy of *PMP22* is not yet clearly defined, it is well established that a correct stoichiometry of PMP22 protein is required to maintain compact myelin integrity [62, 63]. Correction of the PMP22 expression level reverses the demyelination phenotype in a transgenic animal model [64], and the relevance of reducing PMP22 expression has been acknowledged as one potential therapeutic approach for CMT1A [65]. Recently, several approaches aimed at reducing PMP22 mRNA expression, such as anti-sense oligonucleotides (ASO), siRNA and AAV2/9-mediated shRNA targeting PMP22, have been successfully tested in murine models [66–69], but their translation to humans still poses several hurdles.

We reasoned that a pharmacologic approach like IFB-088 aimed at attenuating general protein translation, thus reducing also PMP22 levels, would currently represent a more viable option than gene therapies. For this study, we used the C3-PMP22 mice that carry 3–4 copies of the human *PMP22* gene, and that is thought to represent the more appropriate model to study CMT1A, as compared to C22 mice (carrying 7–8 copies) [26]. We showed that in C3-PMP22 mice PMP22 overexpression results in the activation of the stress sensor BiP and of the PERK/P-eIF2α pathway of the UPR, which supports the idea that activation of a stress response could be a contributing factor in CMT1A pathogenesis.

IFB-088 Treatment Improves Disease Features in CMT1A Mice

Treatment with IFB-088 improved motor capacity, neurophysiology and peripheral nerve morphology and partially readjusted both myelin protein stoichiometry and stress levels in C3-PMP22 CMT1A mice. Importantly, the treatment

Table 1 Percentage of amyelinated fibres amongst axons with diameter larger than 1 µm. Data were expressed in percentage of fibres as mean ± SEM. $n = 5–8$ mice per condition. $^{**}P < 0.01$ by one-way ANOVA with Tukey post-hoc test; $^{\S}P < 0.05$ by Student's *t*-test vs C3-PMP22 vehicle

		WT vehicle *b.i.d*	C3 vehicle *b.i.d*	C3 IFB-088 0.5 mg/kg *b.i.d*	C3 IFB-088 1 mg/kg *b.i.d*
% of amyelinated fibres	All mice	0.033 ± 0.08	27.2 ± 2.4	**19.9 ± 1.3****	21.9 ± 1.4
	Females	0.1 ± 0.06	29.9 ± 1	19.8 ± 2.5§	23.5 ± 0.3
	Males	0	25.4 ± 3.9	20 ± 1.2	20.3 ± 2.7

was started at PND15, when morphological deficits are already evident and ER stress already activated, indicating that the treatment is ameliorating the disease and not simply preventing it. Intriguingly, some of these improvements were more prominent (treadmill) or present exclusively (neurophysiology) in females, whereas the improvement in dysmyelination was detectable in both sexes although, again, some morphological parameters were ameliorated

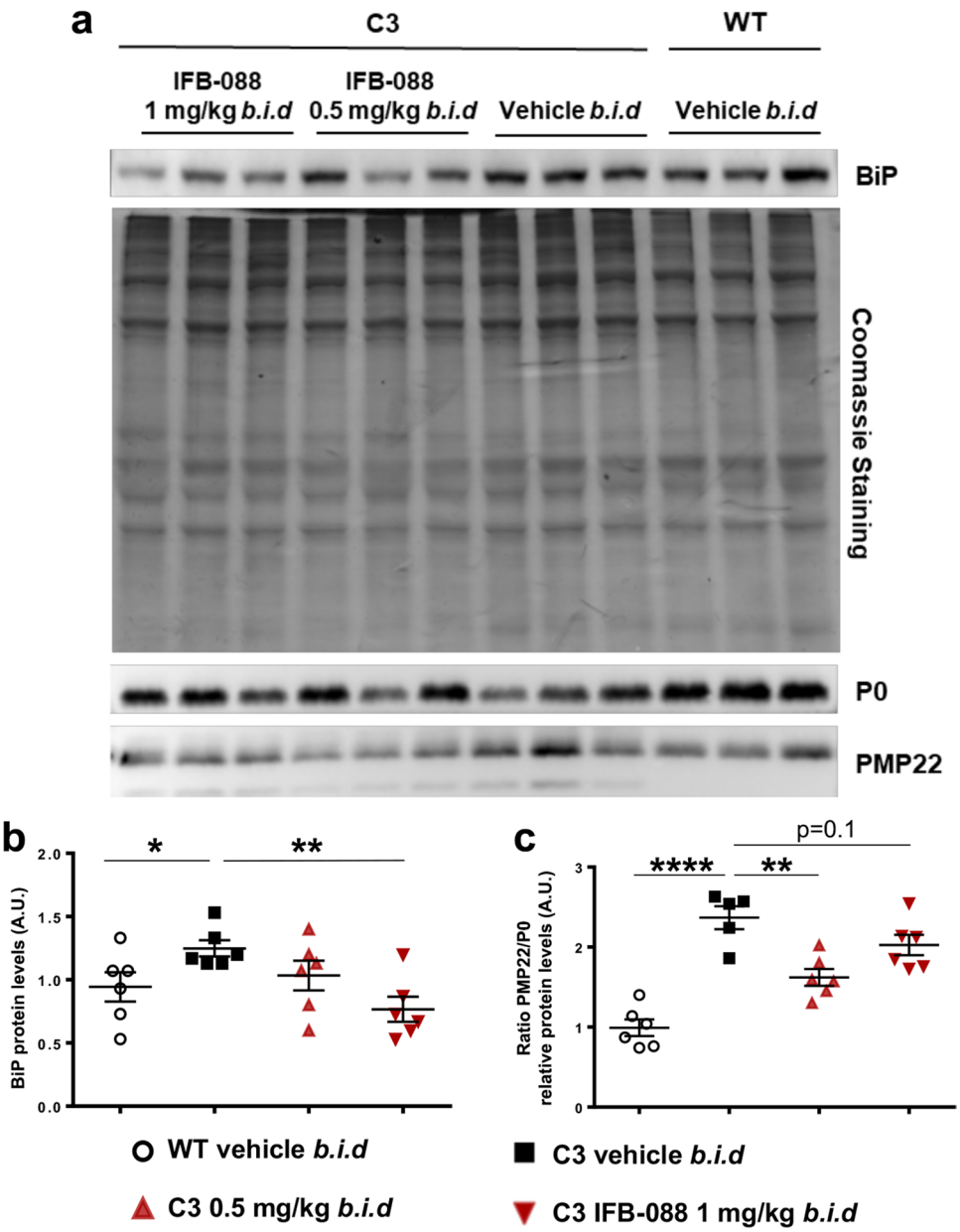

Fig. 7 IFB-088 treatment improves PMP22 stoichiometry in C3-PMP22 mouse peripheral nerves and reduces ER stress. Evaluation of PMP22, P0 and BiP protein levels by WB in sciatic nerve protein lysates from WT mice treated with vehicle *b.i.d.* and C3-PMP22 (C3) mice treated with vehicle *b.i.d.* or IFB-088 at 0.5 or 1 mg/kg *b.i.d.* **a** Representative picture. Three representative samples per condition out of five/six are shown. **b** Quantification of BiP protein level. **c** Quantification of the PMP22/P0 protein ratio. $^{*}P < 0.05$; $^{**}P < 0.01$; $^{****}P < 0.0001$ by Student's *t*-test

more in females than in males. The reasons for these differences are not clear. We ruled out a difference in IFB-088 exposure in males and females, as, in C57BL/6J mice, the same background as the C3-PMP22, no difference in terms of IFB-088 pharmacokinetic profile was observed (Additional File 1: Supplementary Fig. 8). Moreover, we did not detect significant gender differences in the response to treatment in *Mpz*R98C/ + mice (this study), nor in *Mpz*S63del mice [24]. These results suggest that the difference may be more specific to the C3-PMP22 model itself. Of note, differences in motor capacity between genders have already been observed in different experimental settings in C3-PMP22 mice (F. Baas, *unpublished*) and in rotarod in the C22 model, with males performing significantly worse than females [70].

Neurophysiology analysis revealed an amelioration in nerve conduction velocity exclusively in females. The strong neurophysiological impairment in C3-PMP22 mice was accompanied by a complex and severe dysmyelinating phenotype, characterized by hypermyelination of small fibres and almost complete amyelination of large fibres, consistent with previous reports [26]. While myelination of large fibres improved almost equally in males and females after treatment with IFB-088, small-fibre hypermyelination was more efficiently corrected in females. Whether this difference in morphological rescue is sufficient to explain the discrepancy in NCV after treatment remains unclear, however, as the speed of NCV depends predominantly on large-diameter fibres [71].

The dysmyelinating phenotype in C3-PMP22 mice was accompanied by an increase in the levels of the ER-stress markers BiP and of P-eIF2α. Conversely, *Xbp1s* levels did not change significantly between WT and C3-PMP22 nerves, indicating that, unlike the CMT1B models *Mpz*R98C/ + and *Mpz*S63del, not all the UPR pathways were activated by PMP22 overexpression. This difference is likely related to different mechanisms of stress activation in the two models: whereas R98C and Ser63del P0 are misfolded proteins retained in the ER [22, 23, 29] where they activate a canonical UPR, overexpression of PMP22 is thought to overwhelm the ERAD-proteasome system, and the activation of ER stress is likely a secondary event. In this respect, it has been shown that ERAD impairment in Schwann cells results in ER-stress activation [50, 72]. We hypothesize that by prolonging the phosphorylation of eIF2α, IFB-088 attenuates the translational of highly expressed myelin proteins including PMP22. As a result, stress levels were restored towards WT levels in treated C3-PMP22 mice, and there was a partial readjustment of protein stoichiometry in nerves from both male and female mice.

Despite these very promising results, C3-PMP22 was only partially improved, and not fully rescued, probably because, as for *MPZ*R98C/ + mice, the dysmyelinating phenotype of these mice is very severe to start with. Several questions remain to be answered, including whether a prolonged treatment beyond 4 months of age would further improve the phenotype, and whether a treatment initiated in adult mice would still provide benefits. Moreover, it should be noted that while the C3-PMP22 mouse represents a good model of CMT1A, currently there is no authentic animal model for this disease, as all available models express extra copies of the *PMP22* gene but without replicating the 1.4-Mb duplication found in humans.

In summary, we have demonstrated that IFB-088 treatment improved the neuropathy in *Mpz*R98C/ + mice, a CMT1B mouse model, and in C3-PMP22 mice, a CMT1A mouse model. This is the second example of IFB-088's ability to improve the neuropathy in a mouse model of CMT1B. We have identified many additional mutations in *MPZ* that activate the UPR [20] and expect that IFB-088 may prove beneficial in many of these patients. In addition, our study confirms a role of ER stress in the pathogenesis of CMT1A and demonstrate the ability of IFB-088 to assist the ER-stress response to the over-expression of PMP22 and potentially treat patients with CMT1A. Thus, IFB-088, which completed successfully the phase I clinical trial, represents a new and promising therapeutic option for CMT1A and CMT1B. Due to this mode of action, IFB-088 has the unique potential to provide benefits to different CMT subtypes caused by different gene defects. Moreover, the benefits of IFB-088 have also been demonstrated in amyotrophic lateral sclerosis and in multiple sclerosis models [24, 73, 74], suggesting that managing UPR and ER stress is a promising strategy for multiple neurodegenerative diseases.

Supplementary Information The online version contains supplementary material available at https://doi.org/10.1007/s12035-022-02838-y.

Acknowledgements We thank the Charcot-Marie-Tooth Association for its continuous support. We are grateful to Dr. Patrizia D'Adamo and the Mouse Behaviour Facility at IRCCS Ospedale San Raffaele. Part of this work was carried out in ALEMBIC, an advanced microscopy laboratory established by IRCCS Ospedale San Raffaele and Università Vita-Salute San Raffaele. M.D. is supported by Fondazione Telethon (GGP19099), CMTA (Charcot-Marie-Tooth Association, USA) and CMTRF (Charcot-Marie-Tooth Research Foundation).

Author Contribution M.D., M.E.S., P.G., P.M., C.T. contributed to the study conception and design. F.B. provided the C3-PMP22 mouse model. R.M. performed the myelinating DRG explant cultures. Y.B. and DW performed the study in the MpzR98C/ + mouse model. V.G.V., C.S., C.F., R.M., T.T. and F.F. performed the study in the C3-PMP22 mouse model. F.B. and U.D. performed the neurophysiological evaluation of the C3-PMP22 mice. M.D., M.E.S. and C.T. wrote the manuscript. All authors commented on previous versions of the manuscript. All authors read and approved the final manuscript.

Funding This work was funded by InFlectis BioScience.

Data Availability The data that support the findings of this study are available from the corresponding author, upon reasonable request.

Declarations

Ethics Approval All experiments involving animals were performed in accord with experimental protocols approved by the San Raffaele Scientific Institute and the University of Iowa Animal Care and Use Committee.

Consent to Participate Not applicable.

Consent for Publication Not applicable.

Competing Interests P.G., P.M. and C.T. are full-time employees and stockholders of InFlectis BioScience. M.D. acts as a Scientific Advisory Board member and Consultant for InFlectis BioScience.

References

1. Skre H (1974) Genetic and clinical aspects of Charcot-Marie-Tooth's disease. Clin Genet 6:98–118
2. Fridman V, Bundy B, Reilly MM, Pareyson D, Bacon C, Burns J, Day J, Feely S et al (2015) CMT subtypes and disease burden in patients enrolled in the Inherited Neuropathies Consortium natural history study: a cross-sectional analysis. J Neurol Neurosurg Psychiatry 86:873–878
3. Murphy SM, Laura M, Fawcett K, Pandraud A, Liu YT, Davidson GL, Rossor AM, Polke JM et al (2012) Charcot-Marie-Tooth disease: frequency of genetic subtypes and guidelines for genetic testing. J Neurol Neurosurg Psychiatry 83:706–710
4. Lupski JR, de Oca-Luna RM, Slaugenhaupt S, Pentao L, Guzzetta V, Trask BJ, Saucedo-Cardenas O, Barker DF et al (1991) DNA duplication associated with Charcot-Marie-Tooth disease type 1A. Cell 66:219–232
5. Timmerman V, Nelis E, Van Hul W, Nieuwenhuijsen BW, Chen KL, Wang S, Ben Othman K, Cullen B et al (1992) The peripheral myelin protein gene PMP-22 is contained within the Charcot-Marie-Tooth disease type 1A duplication. Nat Genet 1:171–175
6. Hayasaka K, Ohnishi A, Takada G, Fukushima Y, Murai Y (1993) Mutation of the myelin P0 gene in Charcot-Marie-tooth neuropathy type 1. Biochem Biophys Res Commun 194:1317–1322
7. Pareek S, Notterpek L, Snipes GJ, Naef R, Sossin W, Laliberte J, Iacampo S, Suter U et al (1997) Neurons promote the translocation of peripheral myelin protein 22 into myelin. J Neurosci 17:7754–7762
8. Anelli T, Sitia R (2008) Protein quality control in the early secretory pathway. EMBO J 27:315–327
9. Fortun J, Go JC, Li J, Amici SA, Dunn WA Jr, Notterpek L (2006) Alterations in degradative pathways and protein aggregation in a neuropathy model based on PMP22 overexpression. Neurobiol Dis 22:153–164
10. Lee S, Bazick H, Chittoor-Vinod V, Al Salihi MO, Xia G, Notterpek L (2018) Elevated peripheral myelin protein 22, reduced mitotic potential, and proteasome impairment in dermal fibroblasts from Charcot-Marie-Tooth disease type 1A patients. Am J Pathol 188:728–738
11. Notterpek L, Ryan MC, Tobler AR, Shooter EM (1999) PMP22 accumulation in aggresomes: implications for CMT1A pathology. Neurobiol Dis 6:450–460
12. Schlebach JP, Peng D, Kroncke BM, Mittendorf KF, Narayan M, Carter BD, Sanders CR (2013) Reversible folding of human peripheral myelin protein 22, a tetraspan membrane protein. Biochemistry 52:3229–3241
13. Harding HP, Zhang Y, Bertolotti A, Zeng H, Ron D (2000) Perk is essential for translational regulation and cell survival during the unfolded protein response. Mol Cell 5:897–904
14. Lin JH, Li H, Zhang Y, Ron D, Walter P (2009) Divergent effects of PERK and IRE1 signaling on cell viability. PLoS One 4:e4170
15. Ha N, Choi YI, Jung N, Song JY, Bae DK, Kim MC, Lee YJ, Song H et al (2020) A novel histone deacetylase 6 inhibitor improves myelination of Schwann cells in a model of Charcot-Marie-Tooth disease type 1A. Br J Pharmacol 177:5096–5113
16. Okamoto Y, Pehlivan D, Wiszniewski W, Beck CR, Snipes GJ, Lupski JR, Khajavi M (2013) Curcumin facilitates a transitory cellular stress response in Trembler-J mice. Hum Mol Genet 22:4698–4705
17. Khajavi M, Shiga K, Wiszniewski W, He F, Shaw CA, Yan J, Wensel TG, Snipes GJ et al (2007) Oral curcumin mitigates the clinical and neuropathologic phenotype of the Trembler-J mouse: a potential therapy for inherited neuropathy. Am J Hum Genet 81:438–453
18. Sanmaneechai O, Feely S, Scherer SS, Herrmann DN, Burns J, Muntoni F, Li J, Siskind CE et al (2015) Genotype-phenotype characteristics and baseline natural history of heritable neuropathies caused by mutations in the MPZ gene. Brain 138:3180–3192
19. Grandis M, Vigo T, Passalacqua M, Jain M, Scazzola S, La Padula V, Brucal M, Benvenuto F et al (2008) Different cellular and molecular mechanisms for early and late-onset myelin protein zero mutations. Hum Mol Genet 17:1877–1889
20. Bai Y, Wu X, Brennan KM, Wang DS, D'Antonio M, Moran J, Svaren J, Shy ME (2018) Myelin protein zero mutations and the unfolded protein response in Charcot Marie Tooth disease type 1B. Ann Clin Transl Neurol 5:445–455
21. Khajavi M, Inoue K, Wiszniewski W, Ohyama T, Snipes GJ, Lupski JR (2005) Curcumin treatment abrogates endoplasmic reticulum retention and aggregation-induced apoptosis associated with neuropathy-causing myelin protein zero-truncating mutants. Am J Hum Genet 77:841–850
22. Pennuto M, Tinelli E, Malaguti M, Del Carro U, D'Antonio M, Ron D, Quattrini A, Feltri ML et al (2008) Ablation of the UPR-Mediator CHOP Restores Motor Function and Reduces Demyelination in Charcot-Marie-Tooth 1B Mice. Neuron 57:393–405
23. Saporta MA, Shy BR, Patzko A, Bai Y, Pennuto M, Ferri C, Tinelli E, Saveri P et al (2012) MpzR98C arrests Schwann cell development in a mouse model of early-onset Charcot-Marie-Tooth disease type 1B. Brain 135:2032–2047
24. Das I, Krzyzosiak A, Schneider K, Wrabetz L, D'Antonio M, Barry N, Sigurdardottir A, Bertolotti A (2015) Preventing proteostasis diseases by selective inhibition of a phosphatase regulatory subunit. Science 348:239–242. https://doi.org/10.1126/science.aaa4484
25. Fledrich R, Stassart RM, Sereda MW (2012) Murine therapeutic models for Charcot-Marie-Tooth (CMT) disease. Br Med Bull 102:89–113

26. Verhamme C, King RH, ten Asbroek AL, Muddle JR, Nourallah M, Wolterman R, Baas F, van Schaik IN (2011) Myelin and axon pathology in a long-term study of PMP22-overexpressing mice. J Neuropathol Exp Neurol 70:386–398
27. Taveggia C, Zanazzi G, Petrylak A, Yano H, Rosenbluth J, Einheber S, Xu X, Esper RM et al (2005) Neuregulin-1 type III determines the ensheathment fate of axons. Neuron 47:681–694
28. D'Antonio M, Musner N, Scapin C, Ungaro D, Del Carro U, Ron D, Feltri ML, Wrabetz L (2013) Resetting translational homeostasis restores myelination in Charcot-Marie-Tooth disease type 1B mice. J Exp Med 210:821–838
29. Wrabetz L, D'Antonio M, Pennuto M, Dati G, Tinelli E, Fratta P, Previtali S, Imperiale D et al (2006) Different intracellular pathomechanisms produce diverse Myelin Protein Zero neuropathies in transgenic mice. J Neurosci 26:2358–2368
30. Takeo T, Nakagata N (2011) Reduced glutathione enhances fertility of frozen/thawed C57BL/6 mouse sperm after exposure to methyl-beta-cyclodextrin. Biol Reprod 85:1066–1072
31. Biffi A, De Palma M, Quattrini A, Del Carro U, Amadio S, Visigalli I, Sessa M, Fasano S et al (2004) Correction of metachromatic leukodystrophy in the mouse model by transplantation of genetically modified hematopoietic stem cells. J Clin Invest 113:1118–1129
32. Lancaster E, Li J, Hanania T, Liem R, Scheideler MA, Scherer SS (2018) Myelinated axons fail to develop properly in a genetically authentic mouse model of Charcot-Marie-Tooth disease type 2E. Exp Neurol 308:13–25
33. Ferri C, Quattrini A, D'Antonio M (2018) Electron microscopy for the analysis of peripheral nerve myelin. Methods Mol Biol 1791:3–13
34. Patzko A, Bai Y, Saporta MA, Katona I, Wu X, Vizzuso D, Feltri ML, Wang S et al (2012) Curcumin derivatives promote Schwann cell differentiation and improve neuropathy in R98C CMT1B mice. Brain 135:3551–3566
35. Wrabetz L, Feltri ML, Quattrini A, Imperiale D, Previtali S, D'Antonio M, Martini R, Yin X et al (2000) P(0) glycoprotein overexpression causes congenital hypomyelination of peripheral nerves. J Cell Biol 148:1021–1034
36. D'Antonio M, Michalovich D, Paterson M, Droggiti A, Woodhoo A, Mirsky R, Jessen KR (2006) Gene profiling and bioinformatic analysis of Schwann cell embryonic development and myelination. Glia 53:501–515
37. Parkinson DB, Bhaskaran A, Arthur-Farraj P, Noon LA, Woodhoo A, Lloyd AC, Feltri ML, Wrabetz L et al (2008) c-Jun is a negative regulator of myelination. J Cell Biol 181:625–637
38. Hantke J, Carty L, Wagstaff LJ, Turmaine M, Wilton DK, Quintes S, Koltzenburg M, Baas F et al (2014) c-Jun activation in Schwann cells protects against loss of sensory axons in inherited neuropathy. Brain 137:2922–2937
39. Volpi VG, Touvier T, D'Antonio M (2017) Endoplasmic reticulum protein quality control failure in myelin disorders. Front Mol Neurosci 9:162
40. Bai Y, Ianokova E, Pu Q, Ghandour K, Levinson R, Martin JJ, Ceuterick-de Groote C et al (2006) Effect of an R69C mutation in the myelin protein zero gene on myelination and ion channel subtypes. Arch Neurol 63:1787–1794
41. Miller LJ, Patzko A, Lewis RA, Shy ME (2012) Phenotypic presentation of the Ser63Del MPZ mutation. J Peripher Nerv Syst 17:197–200
42. Shapiro L, Doyle JP, Hensley P, Colman DR, Hendrickson WA (1996) Crystal structure of the extracellular domain from P0, the major structural protein of peripheral nerve myelin. Neuron 17:435–449
43. Avila RL, D'Antonio M, Bachi A, Inouye H, Feltri ML, Wrabetz L, Kirschner DA (2010) P0 (protein zero) mutation S34C underlies instability of internodal myelin in S63C mice. J Biol Chem 285:42001–42012
44. Monk KR, Feltri ML, Taveggia C (2015) New insights on Schwann cell development. Glia 63:1376–1393
45. Nave KA (2010) Myelination and support of axonal integrity by glia. Nature 468:244–252
46. Greenfield S, Brostoff S, Eylar EH, Morell P (1973) Protein composition of myelin of the peripheral nervous system. J Neurochem 20:1207–1216
47. Lemke G, Axel R (1985) Isolation and sequence of a cDNA encoding the major structural protein of peripheral myelin. Cell 40:501–508
48. Ellgaard L, Helenius A (2003) Quality control in the endoplasmic reticulum. Nat Rev Mol Cell Biol 4:181–191
49. VerPlank JJS, Lokireddy S, Feltri ML, Goldberg AL, Wrabetz L (2018) Impairment of protein degradation and proteasome function in hereditary neuropathies. Glia 66:379–395
50. Volpi VG, Ferri C, Fregno I, Del Carro U, Bianchi F, Scapin C, Pettinato E, Solda T et al (2019) Schwann cells ER-associated degradation contributes to myelin maintenance in adult nerves and limits demyelination in CMT1B mice. PLoS Genet 15:e1008069
51. VerPlank JJS, Gawron J, Silvestri NJ, Feltri ML, Wrabetz L, Goldberg AL (2021) Raising cGMP restores proteasome function and myelination in mice with a proteotoxic neuropathy. Brain. https://doi.org/10.1093/brain/awab249
52. Florio F, Ferri C, Scapin C, Feltri ML, Wrabetz L, D'Antonio M (2018) Sustained expression of negative regulators of myelination protects Schwann cells from dysmyelination in a Charcot-Marie-Tooth 1B mouse model. J Neurosci 38:4275–4287
53. Howard P, Feely SME, Grider T, Bacha A, Scarlato M, Fazio R, Quattrini A, Shy ME et al (2021) Loss of Function MPZ Mutation causes milder CMT1B Neuropathy. J Peripher Nerv Syst 26:177–183
54. Huxley C, Passage E, Manson A, Putzu G, Figarella-Branger D, Pellissier JF, Fontes M (1996) Construction of a mouse model of Charcot-Marie-Tooth disease type 1A by pronuclear injection of human YAC DNA. Hum Mol Genet 5:563–569
55. Sereda M, Griffiths I, Puhlhofer A, Stewart H, Rossner MJ, Zimmerman F, Magyar JP, Schneider A et al (1996) A transgenic rat model of Charcot-Marie-Tooth disease. Neuron 16:1049–1060
56. Pareek S, Suter U, Snipes GJ, Welcher AA, Shooter EM, Murphy RA (1993) Detection and processing of peripheral myelin protein PMP22 in cultured Schwann cells. J Biol Chem 268:10372–10379
57. Marinko JT, Carter BD, Sanders CR (2020) Direct relationship between increased expression and mistrafficking of the Charcot-Marie-Tooth-associated protein PMP22. J Biol Chem 295:11963–11970
58. Katona I, Wu X, Feely SM, Sottile S, Siskind CE, Miller LJ, Shy ME, Li J (2009) PMP22 expression in dermal nerve myelin from patients with CMT1A. Brain 132:1734–1740
59. Li J, Bai Y, Ghandour K, Qin P, Grandis M, Trostinskaia A, Ianakova E, Wu X et al (2005) Skin biopsies in myelin-related neuropathies: bringing molecular pathology to the bedside. Brain 128:1168–1177
60. Gabriel JM, Erne B, Pareyson D, Sghirlanzoni A, Taroni F, Steck AJ (1997) Gene dosage effects in hereditary peripheral neuropathy. Expression of peripheral myelin protein 22 in Charcot-Marie-Tooth disease type 1A and hereditary neuropathy with liability to pressure palsies nerve biopsies. Neurology 49:1635–1640
61. Vallat JM, Sindou P, Preux PM, Tabaraud F, Milor AM, Couratier P, LeGuern E, Brice A (1996) Ultrastructural PMP22 expression in inherited demyelinating neuropathies. Ann Neurol 39:813–817
62. Hirt N, Eggermann K, Hyrenbach S, Lambeck J, Busche A, Fischer J, Rudnik-Schoneborn S, Gaspar H (2015) Genetic dosage compensation via co-occurrence of PMP22 duplication and PMP22 deletion. Neurology 84:1605–1606

63. Huxley C, Passage E, Robertson AM, Youl B, Huston S, Manson A, Saberan-Djoniedi D, Figarella-Branger D et al (1998) Correlation between varying levels of PMP22 expression and the degree of demyelination and reduction in nerve conduction velocity in transgenic mice. Hum Mol Genet 7:449–458
64. Perea J, Robertson A, Tolmachova T, Muddle J, King RH, Ponsford S, Thomas PK, Huxley C (2001) Induced myelination and demyelination in a conditional mouse model of Charcot-Marie-Tooth disease type 1A. Hum Mol Genet 10:1007–1018
65. Pantera H, Shy ME, Svaren J (2020) Regulating PMP22 expression as a dosage sensitive neuropathy gene. Brain Res 1726:146491. https://doi.org/10.1016/j.brainres.2019.146491
66. Boutary S, Caillaud M, El Madani M, Vallat JM, Loisel-Duwattez J, Rouyer A, Richard L, Gracia C et al (2021) Squalenoyl siRNA PMP22 nanoparticles are effective in treating mouse models of Charcot-Marie-Tooth disease type 1 A. Commun Biol 4:317
67. Boutary S, Echaniz-Laguna A, Adams D, Loisel-Duwattez J, Schumacher M, Massaad C, Massaad-Massade L (2021) Treating PMP22 gene duplication-related Charcot-Marie-Tooth disease: the past, the present and the future. Trans Res 227:100–111
68. Gautier B, Hajjar H, Soares S, Berthelot J, Deck M, Abbou S, Campbell G, Ceprian M et al (2021) AAV2/9-mediated silencing of PMP22 prevents the development of pathological features in a rat model of Charcot-Marie-Tooth disease 1 A. Nat Commun 12:2356
69. Zhao HT, Damle S, Ikeda-Lee K, Kuntz S, Li J, Mohan A, Kim A, Hung G et al (2018) PMP22 antisense oligonucleotides reverse Charcot-Marie-Tooth disease type 1A features in rodent models. J Clin Investig 128:359–368
70. Passage E, Norreel JC, Noack-Fraissignes P, Sanguedolce V, Pizant J, Thirion X, Robaglia-Schlupp A, Pellissier JF et al (2004) Ascorbic acid treatment corrects the phenotype of a mouse model of Charcot-Marie-Tooth disease. Nat Med 10:396–401
71. Kimura J (2005) Nerve conduction and electromyography. In: Dyck PJ, Thomas PK (eds) Peripheral Neuropathy, 4th ed. Vol. 1. Elsevier/Saunders, Philadelphia, pp 899–970
72. Wu S, Stone S, Yue Y, Lin W (2021) Endoplasmic reticulum associated degradation is required for maintaining endoplasmic reticulum homeostasis and viability of mature Schwann cells in adults. Glia 69:489–506
73. Chen Y, Kunjamma RB, Weiner M, Chan JR, Popko B (2021) Prolonging the integrated stress response enhances CNS remyelination in an inflammatory environment. Elife 10:e65469
74. Chen Y, Podojil JR, Kunjamma RB, Jones J, Weiner M, Lin W, Miller SD, Popko B (2019) Sephin1, which prolongs the integrated stress response, is a promising therapeutic for multiple sclerosis. Brain 142:344–361